



Thermohaline variability and Antarctic bottom water formation at the Ross Sea shelf break

Giorgio Budillon^{a,*}, Pasquale Castagno^{a,b}, Stefano Aliani^c, Giancarlo Spezie^a, Laurie Padman^d

^a Università degli Studi di Napoli "Parthenope", Dipartimento di Scienze per l'Ambiente, Napoli, Italy

^b Università degli Studi di Siena, Scuola di Dottorato in Scienze Polari, Siena, Italy

^c Consiglio Nazionale delle Ricerche, ISMAR, La Spezia, Italy

^d Earth & Space Research, Corvallis, OR, USA

ARTICLE INFO

Article history:

Received 25 January 2011

Received in revised form

14 July 2011

Accepted 18 July 2011

Available online 3 August 2011

Keywords:

Ross Sea

Circulation

Interannual variability

ASF

AABW

HSSW

ISW

ABSTRACT

We use hydrological and current meter data collected in the Ross Sea, Antarctica between 1995 and 2006 to describe the spatial and temporal variability of water masses involved in the production of Antarctic Bottom Water (AABW). Data were collected in two regions of known outflows of dense shelf water in this region; the Drygalski Trough (DT) and the Glomar-Challenger Trough (GCT). Dense shelf water just inshore of the shelf break is dominated by High Salinity Shelf Water (HSSW) in the DT and Ice Shelf Water (ISW) in the GCT. The HSSW in the northern DT freshened by ~ 0.06 in 11 y, while the ISW in the northern GCT freshened by ~ 0.04 in 8 y and warmed by ~ 0.04 °C in 11 y, dominated by a rapid warming during austral summer 2001/02. The Antarctic Slope Front separating the warm Circumpolar Deep Water (CDW) from the shelf waters is more stable near GCT than near DT, with CDW and mixing products being found on the outer DT shelf but not on the outer GCT shelf. The different source waters and mixing processes at the two sites lead to production of AABW with different thermohaline characteristics in the central and western Ross Sea. Multi-year time series of hydrography and currents at long-term moorings within 100 km of the shelf break in both troughs confirm the interannual signals in the dense shelf water and reveal the seasonal cycle of water mass properties. Near the DT the HSSW salinities experienced maxima in March/April and minima in September/October. The ISW in the GCT is warmest in March/April and coolest between August and October. Mooring data also demonstrate significant high-frequency variability associated with tides and other processes. Wavelet analysis of near-bottom moored sensors sampling the dense water cascade over the continental slope west of the GCT shows intermittent energetic pulses of cold, dense water with periods from ~ 32 h to ~ 5 days.

© 2011 Elsevier Ltd. All rights reserved.

1. Introduction

The production of Antarctic Bottom Water (AABW) plays a major role in determining the strength of the global meridional overturning circulation and, therefore, is an important element in the ocean's contribution to global climate (Orsi et al., 2001; Jacobs, 2004; Johnson, 2008). The total production rate of AABW is estimated at ~ 8 Sv (Orsi et al., 2002), with about 50% coming from the Weddell Sea, 25% from the Ross Sea, and the remainder from smaller sources including the Adélie Land coast and Prydz Bay. Recent observations along the Antarctic continental shelves, while discontinuous and sparse, show that AABW has declined in salinity in recent decades, highlighting the importance of continuously monitoring the regions

of major AABW outflows (Robertson et al., 2002; Jacobs, 2004; Smedsrud, 2005; Aoki et al., 2005; Rintoul, 2007; Ozaki et al., 2009).

The production of AABW is the end result of a complex sequence of processes; see, e.g., Stacey and Bowen (1988), Baines and Condie (1998) and Shapiro et al. (2003). First, dense water is formed on the shelf through cooling and salinization during sea ice formation and accumulates as exchange with the deep ocean is impeded by potential vorticity constraints and the presence of a strong density front (the Antarctic Slope Front, or ASF) near the continental shelf break. Second, dense water that does reach north of the shelf break accelerates rapidly downslope under the influence of gravity, possibly aided by thermobaricity. Third, the density flow turns left (in the Southern Hemisphere) due to Coriolis, roughly following the isobaths along the continental slope but still with a significant downslope component; see, e.g., Killworth (1977). Entrainment of the surrounding ocean into the turbulent benthic outflow of dense water during these three stages can significantly change the thermohaline characteristics and density of the outflow. Finally,

* Corresponding author. Tel.: +39 081 5476584; fax: +39 081 5476515.
E-mail address: giorgio.budillon@uniparthenope.it (G. Budillon).

the descending water spreads along isopycnals off the slope, or along the seabed if the outflow is still sufficiently dense. For a general overview of density outflow dynamics and a broader view of global dense water outflows, see Legg et al. (2009).

Along the Antarctic continental shelves the characteristics of water masses involved in each of these stages vary considerably from one location to another, being modified by factors such as the residence time of shelf waters, contributions from basal melting of ice shelves, tidal forcing, flow interactions with bathymetry, nonlinear equation-of-state effects such as thermobaricity, and the properties and stability of the ASF, if present (see, e.g., Gordon, 1974; Gordon et al., 2009a; Shapiro and Hill, 1997; Shapiro et al., 2003; Whitworth et al., 1998; Whitworth and Orsi, 2006; Fahrbach et al., 2001; Ivanov et al., 2004; Jacobs, 2004; Padman et al., 2009). This complexity explains the heterogeneous production of AABW around Antarctica which, in turn, complicates attempts to represent Antarctica's influence on the global ocean.

While we now have a reasonable conceptual understanding of AABW production, further progress is hampered by a paucity of data due, in part, to the wide range of time and space scales of the relevant phenomena. Temporal scales vary from tidal (Whitworth and Orsi, 2006; Padman et al., 2009) to interdecadal (e.g., Jacobs et al., 2002; Jacobs and Guilivi, 2010). Spatial scales vary from less than the Rossby radius ($R_o \approx 5$ km in the Ross Sea) – see, e.g., Muench et al. (2009b) – to the regional scales over which HSSW and ISW are produced. Progress is also hampered by the logistic difficulty of accessing many sites where high AABW production occurs.

Studies over the last decade in the Ross Sea, however, have provided significant new insights into AABW formation from investigations of source water production and variability to the dynamics of dense outflows. The Ross Sea is an excellent place to study these phenomena because areas with all the relevant characteristics can be relatively easily accessed, and there is now a significant database of hydrographic and tracer data from the Ross Sea continental shelf. These data are sufficient to demonstrate significant temporal variability in properties of the water masses in the southern Ross Sea region from 1960 to 2000, with the HSSW freshening by > 0.1 during this period (Jacobs et al., 2002). Using a shorter data set acquired at the end of the 1990s, Budillon and Spezie (2000) found a similar rate of freshening in the deep water in the Terra Nova Bay (TNB) Polynya in the western Ross Sea, where the densest HSSW is formed through intense air/sea interaction. Smethie and Jacobs (2005) also found variability of ISW outflow from the Ross Ice Shelf, based on hydrographic and tracer chemistry data along the Ross Ice Shelf front during three cruises between 1984 and 2000.

Detailed studies in the northwest Ross Sea during the U.S. Antarctic Slope (“AnSlope”) and Italian “CLIMA” programs (Gordon et al., 2009b) have also demonstrated the sensitivity of AABW properties and volume flux to processes acting at short time and space scales. It is now clear that tidal mixing and advection play critical roles in AABW formation (Whitworth and Orsi, 2006; Muench et al., 2009a; Padman et al., 2009; Wang et al., 2010), while processes associated with small-scale bathymetric features assist the injection of AABW into the deep ocean (Muench et al., 2009b; Padman et al., 2009). These and comparable studies in the AABW density outflow from the Filchner Trough in the southern Weddell Sea (Foldvik et al., 2004; Darelius et al., 2009; Wang et al., 2009) point to a need to better understand the small-scale processes acting near the shelf break.

The studies discussed above motivate our investigation of factors influencing variability of AABW production in the Ross Sea. In this paper we use data collected during five CLIMA austral summer cruises and multi-year time series from moored sensors to

describe the variability of thermohaline structure and currents near the shelf break in the western and central Ross Sea between the 1994/95 and 2005/06 austral summers. This data set allows us to extend the previous AnSlope analyses by providing a much longer time series for investigating seasonal and interannual variability, and allowing a detailed comparison of the source waters and outflows from two major troughs with distinct characteristics.

2. General physical and hydrographic setting

The Ross Sea includes the Ross Ice Shelf (RIS: south of $\sim 78^\circ\text{S}$), a broad continental shelf north of the RIS ice front, and the adjacent deeper ocean. A practical definition of the boundary of the deep Ross Sea is that it encompasses the region extending eastward with the Ross Sea gyre and northward at least to the winter ice edge (Budillon, 2007). The continental shelf (Fig. 1) occupies an area of $\sim 5 \times 10^5$ km², excluding the far southern portion covered by the RIS (also $\sim 5 \times 10^5$ km²). The average depth of the continental shelf is ~ 500 m. The deep water offshore of the continental slope exceeds 3000 m depth (Davey and Nitsche, 2005).

The continental shelf is characterized by several fairly shallow banks, separated by depressions down to ~ 1200 m depth; some of these are deeper than the continental shelf break. Most of these banks and depressions (Drygalski, Joides and Glomar-Challenger troughs; denoted DT, JT and GCT, respectively) have a characteristic SSW/NNE orientation (Fig. 1). The troughs are preferred pathways for warm water masses flowing onto the continental shelf (see, e.g., Dinniman et al., 2003) and for cold, dense water heading towards the shelf break from source regions further south. The most recent CLIMA survey reported herein (austral summer 2005/06) sampled both DT and GCT areas. Transects over the Ross Sea shelf were made perpendicular to the expected flow of water parallel to the banks and troughs. Transects at the shelf break were made perpendicular to isobaths to resolve the ASF and the dense water outflows moving westward after exiting the troughs.

In this work we take advantage of previous studies that defined the hydrographic ranges of the principal water masses in the Ross Sea. We use the definitions recently proposed by Orsi and Wiederwohl (2009), who made a new volumetric census of Ross Sea water masses using both traditional thermohaline parameters (potential temperature θ , and salinity S) and neutral density γ^n (Jackett and McDougall, 1997).

Antarctic Surface Water (AASW; $\gamma^n < 28.00$ kg m⁻³, and $S < 34.30$) occupies the upper ocean and is strongly modified by atmospheric forcing, sea ice formation and melting, and mixing with the waters below the AASW.

Shelf Water (SW) is defined by $\gamma^n > 28.27$ kg m⁻³ and $\theta < -1.85$ °C: SW is found below AASW on the shelf, preferentially in the deep troughs. The AABW is defined by $\gamma^n > 28.27$ kg m⁻³ and $\theta > -1.85$ °C. This threshold of γ^n excludes lighter water that can traverse the sill of the Drake Passage; see, e.g., Orsi et al. (1999, 2002) and Jacobs (2004). Water with the same properties of AABW is called Modified Shelf Water (MSW) when it is found at depths < 700 m.

High Salinity Shelf Water (HSSW; defined as $\gamma^n > 28.27$ kg m⁻³, $\theta \geq -1.85$ °C; $S > 34.7$) is mainly formed in the TNB Polynya by salt release during sea ice formation. From this primary source, HSSW spreads along the seabed, filling the depressions of the Ross Sea (Jacobs et al., 1985; Budillon and Spezie, 2000; Budillon et al., 2003). One branch moves northward along the DT where it reaches the shelf break to contribute to AABW formation through mixing (Jacobs et al., 1985; Rintoul, 1998; Bergamasco et al., 2004; Gordon et al., 2004, 2009a; Budillon et al., 2006). Another branch moves southward under the Ross Ice Shelf. Incorporation of meltwater from the ice shelf base produces water that is potentially supercooled;

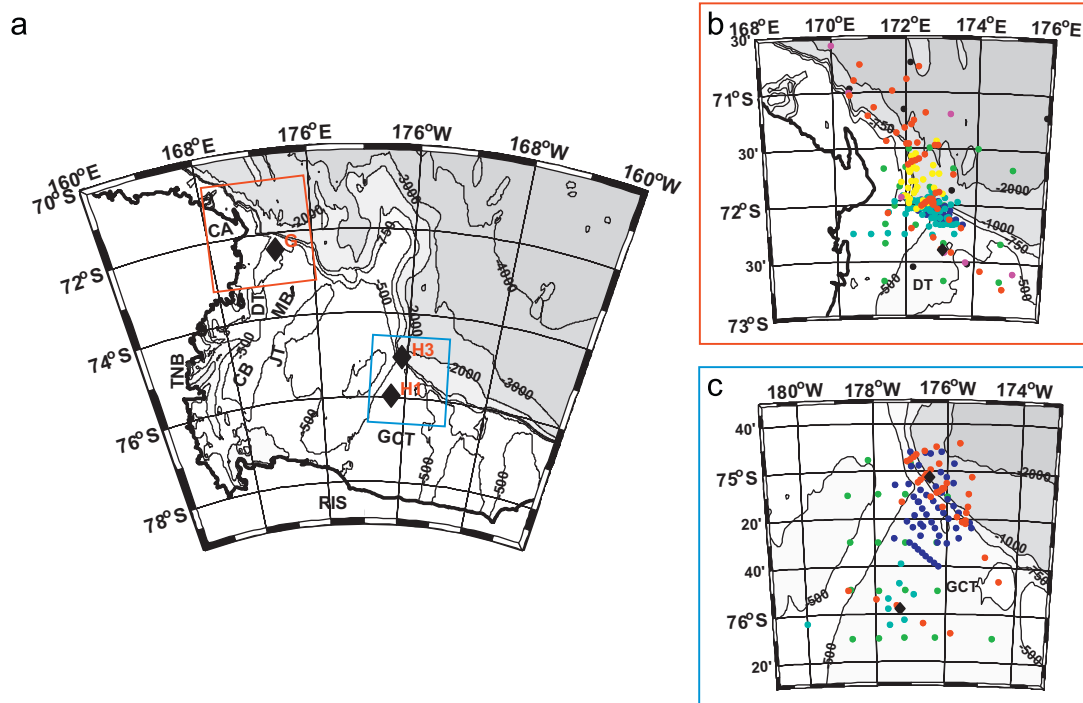


Fig. 1. (a) General map of the Ross Sea with bottom topography in meters and locations of moorings G, H1 and H3 discussed in text. Locations of geographic features discussed in the text are indicated: Terra Nova Bay (TNB), Ross Ice Shelf (RIS), Cape Adare (CA), Drygalski Trough (DT), Glomar-Challenger Trough (GCT), Joides Trough (JT), Mawson Bank (MB) and Cray Bank (CB). CTD/LADCP casts (1994/95 Green, 1997/1998 blue, 1999/2000 black, 2000/01 cyan, 2002/03 yellow, 2003/04 magenta, 2005/06 red) in (b) Drygalski Trough (DT) and (c) Glomar-Challenger Trough (GCT). (For interpretation of the references to color in this figure legend, the reader is referred to the web version of this article.)

i.e., having temperature less than the surface freezing point for the given salinity. This Ice Shelf Water (ISW, $\theta < -1.93^\circ\text{C}$) exits the sub-ice-shelf cavity near the dateline meridian (Smethie and Jacobs, 2005; their Fig. 3) and moves northward along the GCT, reaching the shelf break near 75°S just to the east of the dateline (Jacobs et al., 1985; Trumbore et al., 1991; Holland et al., 2003; Bergamasco et al., 2002a; Budillon et al., 2002a, 2002b; Rubino et al., 2003).

A large volume of Low Salinity Shelf Water (LSSW, defined as $\gamma^n > 28.27\text{ kg m}^{-3}$, $\theta \cong -1.80^\circ\text{C}$; $S \cong 34.47$) is present at intermediate depths in the central eastern Ross Sea (Jacobs et al., 1985; Locarnini, 1994; Russo, 1999; Budillon et al., 2003). Its formation appears to be due to the interaction between AASW and colder waters in the subsurface layers, after several freezing (melting) cycles of the surface water (Jacobs et al., 1985).

Modification of incoming Circumpolar Deep Water (CDW; $\gamma^n > 28.00\text{ kg m}^{-3}$, $\theta > 1.2^\circ\text{C}$) produces Modified Circumpolar Deep Water (MCDW; $28.00 < \gamma^n < 28.27\text{ kg m}^{-3}$). Inflow of MCDW across the continental shelf is the primary source of heat and salt (Jacobs et al., 1985; Budillon et al., 2000b) and nutrients (Smith et al., 2006) to the Ross Sea continental shelf. This inflow appears to be strongly influenced by the topography of the banks and troughs along the shelf break (Dinniman et al., 2003).

3. Data and methods

3.1. Mooring data

Four moorings were deployed near the Ross Sea shelf break for various periods between 1995 and 2008; see Fig. 1 for mooring locations and Fig. 2 for periods of operation. Mooring G (72.39133°S , 173.05628°E) in the DT is close to one deployed for ~ 2 years from 1990 to 1992 (Jaeger et al., 1996). Moorings H1

(75.96158°S , 182.69368°E) and H3 (75.04243°S , 183.51665°E) were deployed in the northern GCT and on the adjacent continental slope, respectively. The fourth mooring, H2, was deployed between H1 and H3 but is not discussed in this paper. The moorings were equipped with current meters, temperature and conductivity sensors, sediment traps and turbidity meters. Aanderaa current meters (models RCM7 and RCM9) were used. The accuracy of the individual speed and direction measurements is $\pm 1\text{ cm s}^{-1}$ and $\pm 5^\circ$, respectively. Systematic errors may occur in the RCM7 time series at very low speeds ($< 1\text{ cm s}^{-1}$); however, measured speeds in the present data set were always well above this threshold level and so we assume errors from this source are negligible. Thermohaline characteristics were measured by SBE-SeaCat 16 and 19 recorders at different depths; accuracy of these sensors was checked against CTD casts before and after deployments.

3.2. Hydrographic data

Hydrographic profiles were collected during five basin-scale surveys from 1994/5 to 2005/06. All surveys (1994/95, 1997/98, 2000/01, 2002/03 and 2005/06) collected data at the northern DT; three surveys (1994/95, 1997/98, and 2005/06) also sampled the northern GCT. Station locations are shown in Fig. 1.

Hydrographic profiles were obtained with a Sea-Bird Electronics SBE 9/11+ coupled to a Carousel water sampler SBE 32 equipped with 24 water-sample bottles of 12 l each. The CTD was equipped with dual temperature-conductivity sensors flushed by pump at a constant rate. Calibrations were performed before and after the cruises. Data were acquired at the maximum frequency (24 Hz) using a PC running DOS/Windows Sea-Bird's Seasave software. Profiles typically reached down to 1–2 m above the seabed. The CTD temperature calibration was checked during cruises with SIS RTM4200 digital reversing platinum thermometers. At every station,

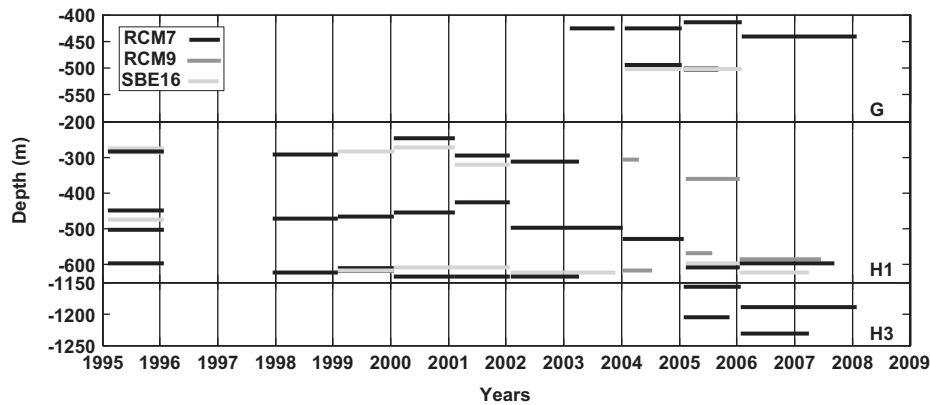


Fig. 2. Operation periods for the moorings deployed in the western and central Ross Sea. The different gray lines indicate the instrument type (see legend, upper right).

several samples of water at different depths and salinity ranges were collected and analyzed on board using an Autosal Guideline salinometer. Typical errors were about ± 0.003 °C for temperature and ± 0.005 for salinity.

Hydrographic data were corrected and processed according to international procedures (UNESCO, 1988). Standard algorithms (UNESCO, 1983) were used to compute quantities such as θ , S and potential density anomaly σ_θ , while γ^n was computed using the Jackett and McDougall (1997) algorithm.

3.3. Velocity profile data

A Lowered Acoustic Doppler Current Profiler (LADCP) was deployed with the CTD during the 2005/06 survey. Two RDI Workhorse 300 kHz ADCP heads in deep pressure housings were mounted on the SBE carousel, one looking upward and the other downward. Both instruments were configured to ping simultaneously at the maximum rate, about three times per second. The bottom-tracking option was also used. Velocity profiles were calculated following the methodology described by Visbeck (2001), using shear estimates from both instruments. For the purposes of this paper we decompose the LADCP current vectors into cross-slope (v_x) and along-slope (v_a) components.

3.4. Wavelet analysis

Oceanographers have traditionally used the Fourier transform to partition the energy of a time series into resolvable frequency bands. However, this approach is appropriate only for stationary signals where all frequencies have an essentially infinite coherence time; e.g., the tidal component of sea surface height variability. Consequently, Fourier analysis cannot detect temporally compact (intermittent or “event-like”) patterns. Since gravity currents are known to be episodic, a different approach is needed to study their temporal variability.

Wavelet analysis is a mathematical method introduced by Morlet et al. (1982) and Morlet (1983) to overcome such disadvantages. Wavelet theory and the application of wavelet analysis to geophysical studies have been widely discussed (e.g., Meyers et al., 1993; Daubechies, 1994; Burrus et al., 1998; Grinsted et al., 2004). The method we use here has been widely used for both oceanographic and meteorological applications with satisfactory results; see, e.g., Foufoula-Georgiou and Kumar (1995). For this paper we use the well-known “Morlet” mother wavelet function, which is defined by

$$\Psi_0(\eta) = \pi^{-1/4} e^{i\omega_0\eta} e^{-(1/2)\eta^2}$$

where ω_0 is dimensionless frequency and η is dimensionless time. When using wavelets for feature extraction purposes, the Morlet wavelet with $\omega_0=6$ is a good choice since it provides a satisfactory balance between time-scale and temporal localization.

4. Results

The two largest sources of AABW leaving the Ross Sea are the DT (western Ross Sea) and GCT (central Ross Sea), corresponding to the pathways of the main outflows of HSSW and ISW, respectively.

4.1. Thermohaline properties at the Drygalski and Glomar-Challenger Troughs (CTD data)

Fig. 3 compares θ/S properties for CTD profiles close to the ASF in the DT and GCT during the 2005/06 CLIMA cruise. The CDW is present in both areas but its θ/S characteristics vary: the CDW core is significantly warmer and has a broader range of salinity near the GCT than in the vicinity of DT. The concavity of the θ/S profiles at depths below the depth of the potential temperature maximum (θ_{\max}) near the DT indicates mixing between CDW and HSSW on the outer shelf. In the GCT region, CDW interacts mainly with ISW.

Comparisons of θ/S properties over the shelf (i.e., with water depth < 700 m) and in the adjacent deep water (Fig. 4) indicate a clear difference between the water masses either side of the ASF at the northern end of the GCT, highlighting the stability of the ASF in this region. Much warmer water is found inshore of the shelf break at the DT, with θ up to $\sim +1$ °C. For shelf water masses ($\gamma^n > 28.27$ kg m $^{-3}$), there is a much broader range of temperature in the DT than in the GCT. The large range of temperature for MSW in the DT indicates significant mixing between the shelf waters and the CDW inshore of the shelf break.

As we will show in Section 4.3.2, regular intrusions of the relatively warm and less oxygenated CDW occur well south of the shelf break in the western sector around DT. These CDW intrusions provide a continuous source for the formation of MCDW ($28.00 < \gamma^n < 28.27$ kg m $^{-3}$) and SW ($\gamma^n > 28.27$ kg m $^{-3}$). In the GCT, in the central sector, there is no clear evidence of intrusions of CDW onto the outer shelf; consequently, the mixing in this region mainly involves ISW and LSSW over the continental slope (see Fig. 3a). (Table 1).

The stations sampled outside the continental shelf (Fig. 4b) show significant differences in the characteristics of the AABW

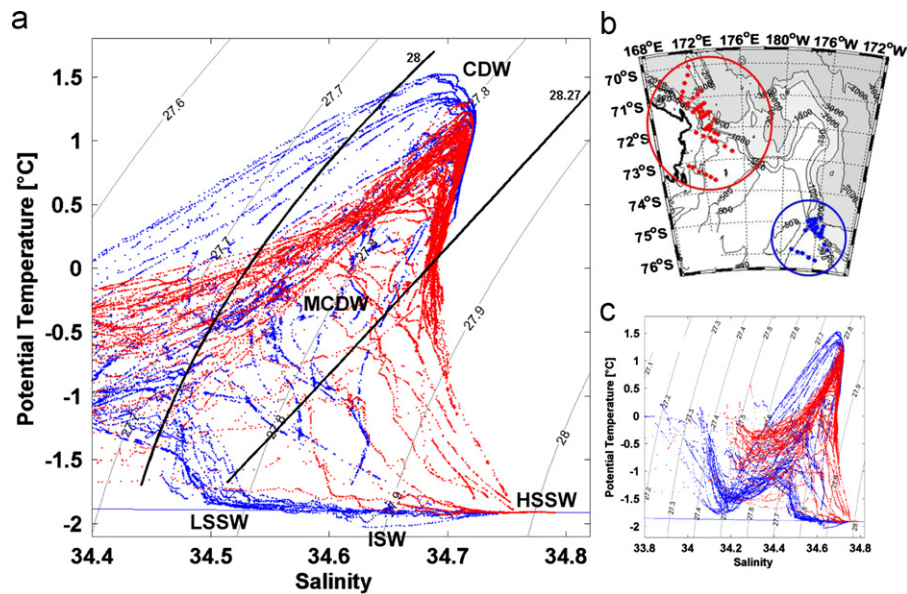


Fig. 3. (a) Zoom of the θ/S scatter plot of all summer 2005/06 casts for the western Ross Sea (red dots) and for the central Ross Sea (blue dots). (b) The position of the casts used in (a). (c) θ/S for the full parameter space. (For interpretation of the references to color in this figure legend, the reader is referred to the web version of this article.)

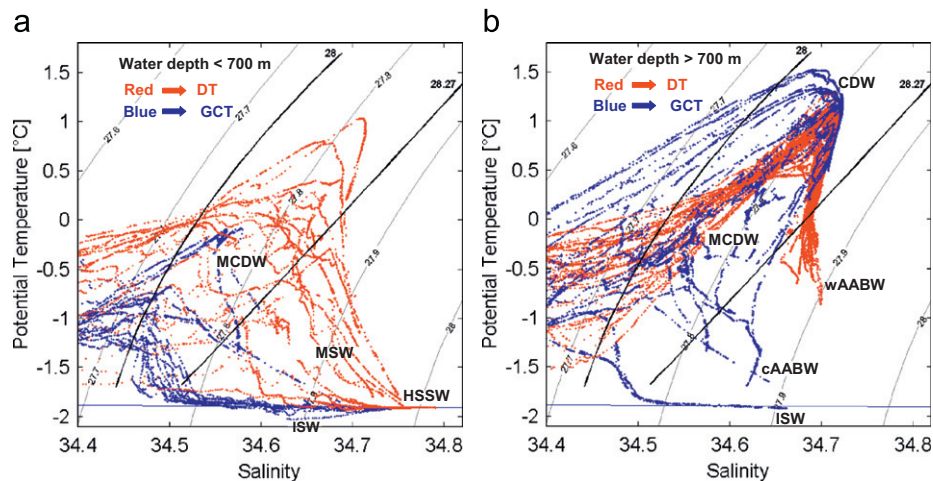


Fig. 4. θ/S scatter plot of summer 2005/06 casts organized by water depth and color coded by western (red) and central (blue) regions (DT and GCT, respectively). (a) Stations sampled over the shelf (depth < 700 m). (b) Stations sampled outside the shelf break (depth > 700 m). (For interpretation of the references to color in this figure legend, the reader is referred to the web version of this article.)

(water with $\gamma^n > 28.27 \text{ kg m}^{-3}$) between the two sectors: the AABW in the western sector is much warmer, saltier and has lower γ^n than in the GCT (see, also, Table 2). The AABW on the slope outside the GCT is strongly influenced by the presence of ISW, similar to the AABW outflow from the Filchner Trough in the southern Weddell Sea (Foldvik et al., 2004; Darelius et al., 2009). The ISW is apparent in Fig. 4b in two casts sampled outside the shelf: cast # 61, bottom depth 760 m, $\theta = -1.922 \text{ }^\circ\text{C}$ at the bottom; and cast # 60, bottom depth 1060 m, $\theta = -1.927 \text{ }^\circ\text{C}$ at the bottom. In both profiles the benthic layer is nearly isothermal over a wide range of salinity. Bergamasco et al. (2002b) documented a similar phenomenon in the same area from data collected during the austral summer 1997/98. Although we collected several CTD profiles on the slope north of the DT in the five surveys, no profiles contained pure shelf water (HSSW), with the coldest benthic water having $\theta > -1 \text{ }^\circ\text{C}$ (Fig. 4b). Sporadic downslope flow events consisting of extremely cold, pure HSSW have been measured by moorings on the slope north

Table 1

CLIMA cruises in the Ross Sea between 1994 and 2006, and number of CTD stations (N_{CTD}).

Cruise	Austral summer	N_{CTD}
PNRA X	1994–1995	154
PNRA XI	1995–1996	38
PNRA XIII	1997–1998	216
PNRA XVI	2000–2001	129
PNRA XVIII	2002–2003	129
PNRA XXI	2005–2006	173

of the DT (Gordon et al., 2004; their Fig. 4) and Muench et al. (2009a; their Fig. 11). However, the duration of each of these events is only a few hours, making them difficult to sample in CTD surveys.

Table 2

Physical properties (potential temperature θ , salinity S and neutral density γ^n) of Antarctic Bottom Water (AABW) formed at the continental slope of the Drygalski Trough (DT) and at the Glomar-Challenger Trough (GCT).

AABW	θ ($^{\circ}\text{C}$)	S	γ^n (kg m^{-3})
DT	-0.75	34.70	28.44
GCT	-1.59	34.63	28.50

The cross-frontal temperature-salinity characteristics of the ASF were further examined using CTD transects perpendicular to the slope during the austral summer 2005/06 CLIMA survey. Examples of these transects for the DT and GCT are shown in Figs. 5 and 6, respectively. Similar results were found for the other CTD transects (not shown here) collected during the 2005/06 cruise. Although the intensity of the ASF varied significantly between the two areas, its location was remarkably constant for different years.

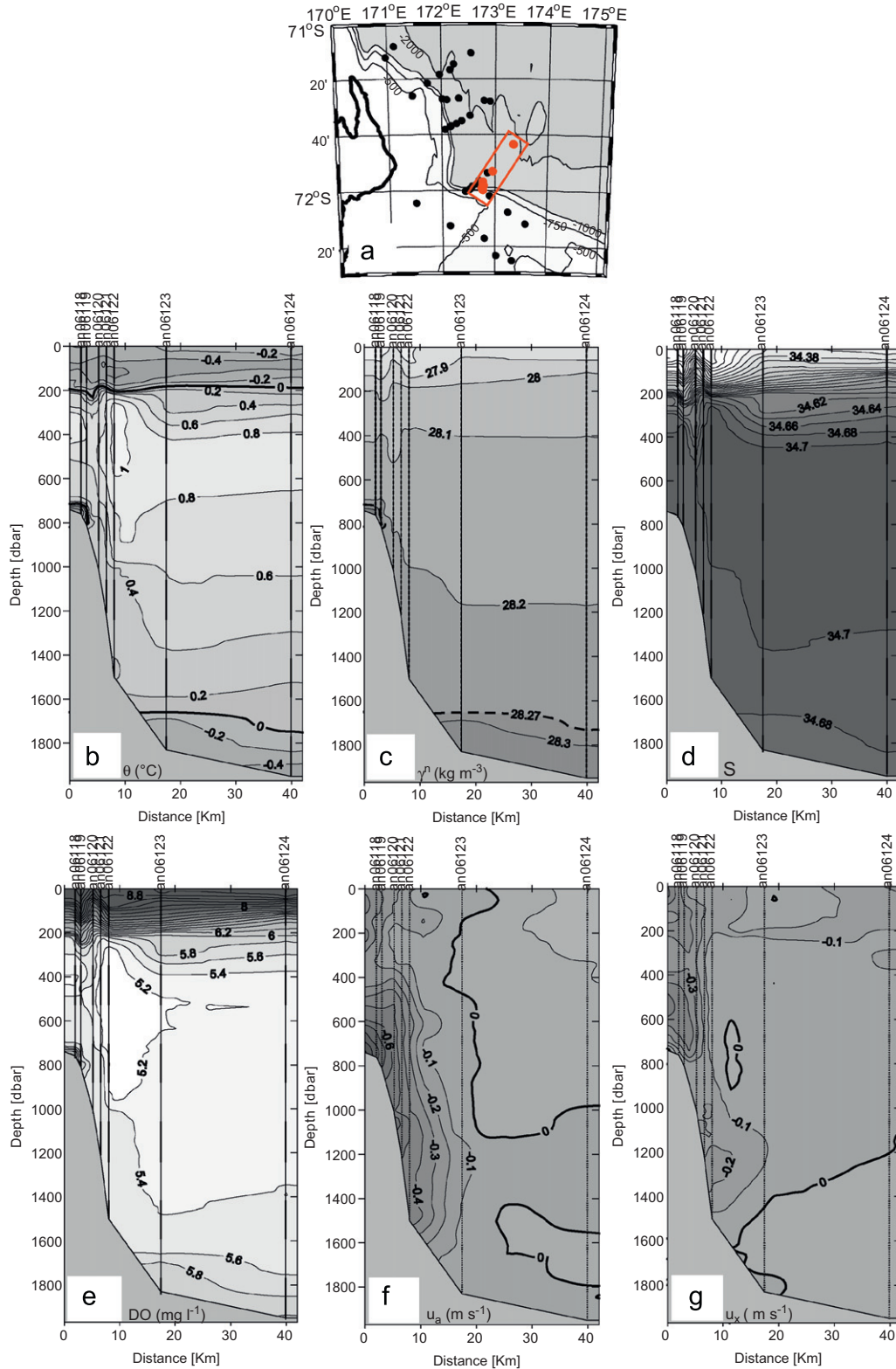


Fig. 5. Vertical section across the continental slope at the Drygalski Trough: (a) transect position; (b) potential temperature θ ($^{\circ}\text{C}$); (c) neutral density γ^n (kg m^{-3}); (d) salinity S ; (e) dissolved oxygen DO (mg l^{-1}); (f) LADCP velocity (m s^{-1}) for the component parallel to the isobaths u_a (positive value: out of the paper); and (g) LADCP velocity component normal to the isobaths u_x (positive values directed offshore).

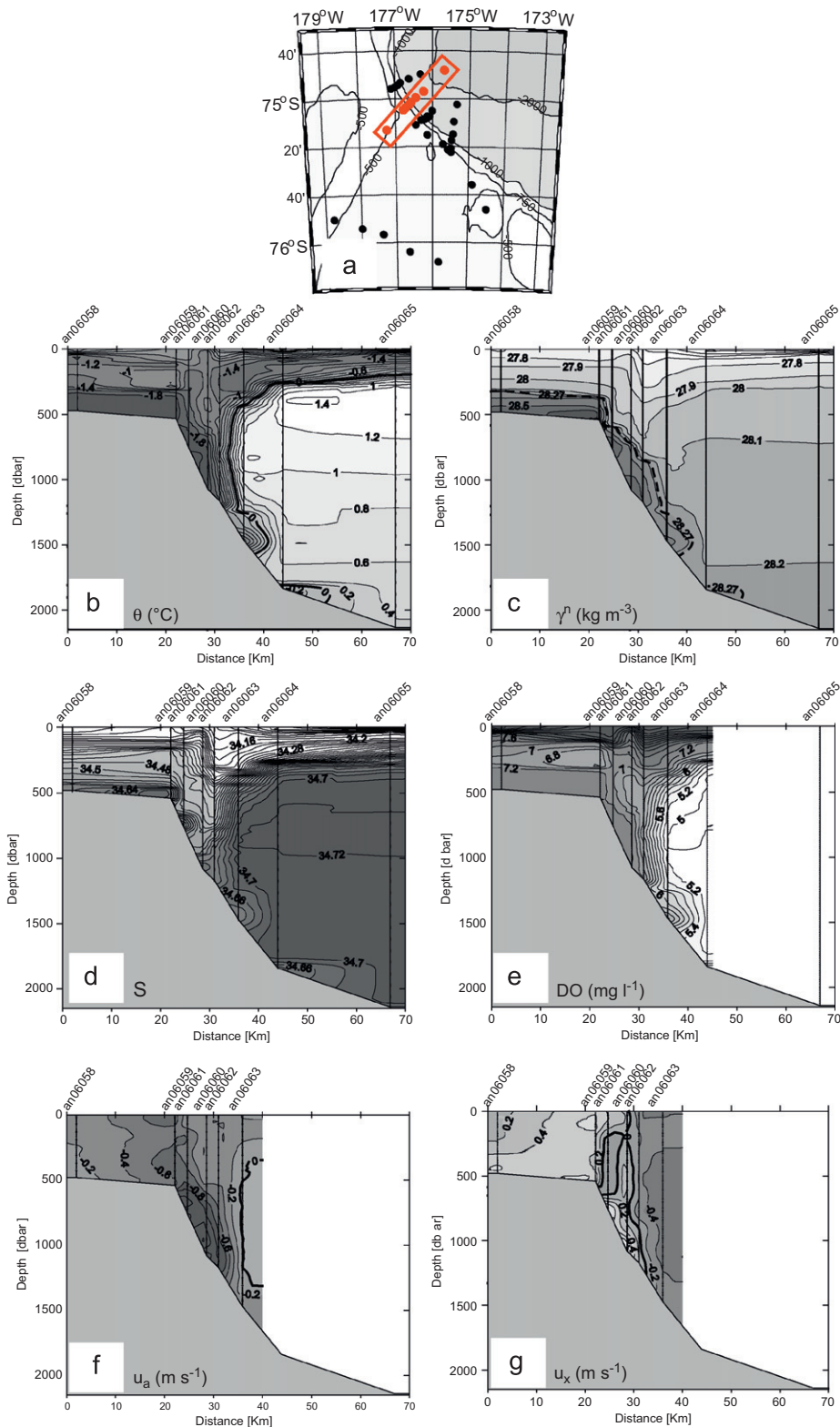


Fig. 6. Vertical section across the continental slope at the Glomar-Challenger Trough: (a) transect position; (b) potential temperature θ (°C); (c) neutral density γ^n (kg m⁻³); (d) salinity S ; (e) dissolved oxygen DO (mg l⁻¹); (f) LADCP velocity (m s⁻¹) for the component parallel to the isobaths u_a (positive value: out of the paper); and (g) LADCP velocity component normal to the isobaths u_x (positive values directed offshore).

At the DT (Fig. 5) a quasi-homogeneous surface layer of AASW was present along the entire section from the continental shelf to the deep water. Over the shelf, MCDW is sandwiched between the AASW and the modified HSSW that occupies the bottom layer; a

similar condition is also detected over the slope where a relatively warm core ($\theta > 1$ °C) identifies the presence of CDW at intermediate depth (250–600 m). Close to the bottom at water depths below ~ 1700 m there is a dense ($\gamma^n > 28.27$ kg m⁻³) and relatively cold

layer indicating the presence of AABW that most likely was formed by the outflow from the eastern basins (Joides Trough and GCT; Gordon et al., 2009a) rather than locally in DT.

Over the shelf at the GCT (Fig. 6), AASW is present in the upper water column and ISW is found close to the bottom. Outside the shelf, the pycnocline separates the AASW from the warmer CDW. Hydrographic measurements show a quasi-continuous benthic layer with $\theta < -1.3$ °C down to the ~ 1500 m isobath (-0.4 °C at a depth of 2000 m). This layer is denser than $\gamma^n = 28.27$ kg m $^{-3}$; i.e., within the range defining AABW (Orsi and Wiederwohl, 2009).

The cross-slope hydrography at GCT (Fig. 6) reveals the classic “V” shaped density field of the ASF (e.g., Ainley and Jacobs, 1981) in the upper ocean and the subsurface front centered over the upper slope. In contrast, the front at DT (Fig. 5), if present at all, is inshore of the shelf break and not sampled in this transect. From previous studies we know that the ASF position is often located over the shelf near the DT (Budillon et al., 2000a; Gordon et al., 2009a), probably due to the large cross-slope displacement (> 10 km) caused by strong tidal currents (Gordon et al., 2009a; Padman et al., 2009).

4.2. LADCP cross-slope sections

Current measurements from the LADCP deployed during the 2005/06 CLIMA cruise in the DT reveal a flow moving roughly

westward from the shelf break (~ 600 m) to depths greater than 1800 m, with speeds > 0.5 m s $^{-1}$ (Fig. 5f). This flow has a significant downslope component of flow over the continental slope (Fig. 5g). However, this region is known to experience significant changes in absolute flow associated with various processes including tides and seasonal variability (Gordon et al., 2009a; Muench et al., 2009a; Padman et al., 2009); thus this single transect cannot be used to infer mean conditions.

A similar velocity transect at the GCT, also from the 2005/06 cruise, shows a cold and high-oxygen plume of ISW leaving the GCT and spilling over the slope. The benthic layer of this energetic gravity current reaches velocities close to 1.2 m s $^{-1}$ in the direction parallel to the isobaths (north-westward) and 0.6 m s $^{-1}$ in the direction normal to the isobaths (north-eastward).

4.3. Seasonal and interannual thermohaline variability in Drygalski and Glomar-Challenger Troughs

4.3.1. CTD data

The CTD profiles at the outflow area of DT near the shelf break were sorted by the year and water depth. Using $S > 34.7$ to define the deeper layer of HSSW in contact with the bottom, we detected a clear reduction in layer-averaged salinity from 1995 up to 2006 (Fig. 7). This value decreases by about 0.06 in these 11 years, with a corresponding decrease in γ^n of ~ 0.2 kg m $^{-3}$. We found

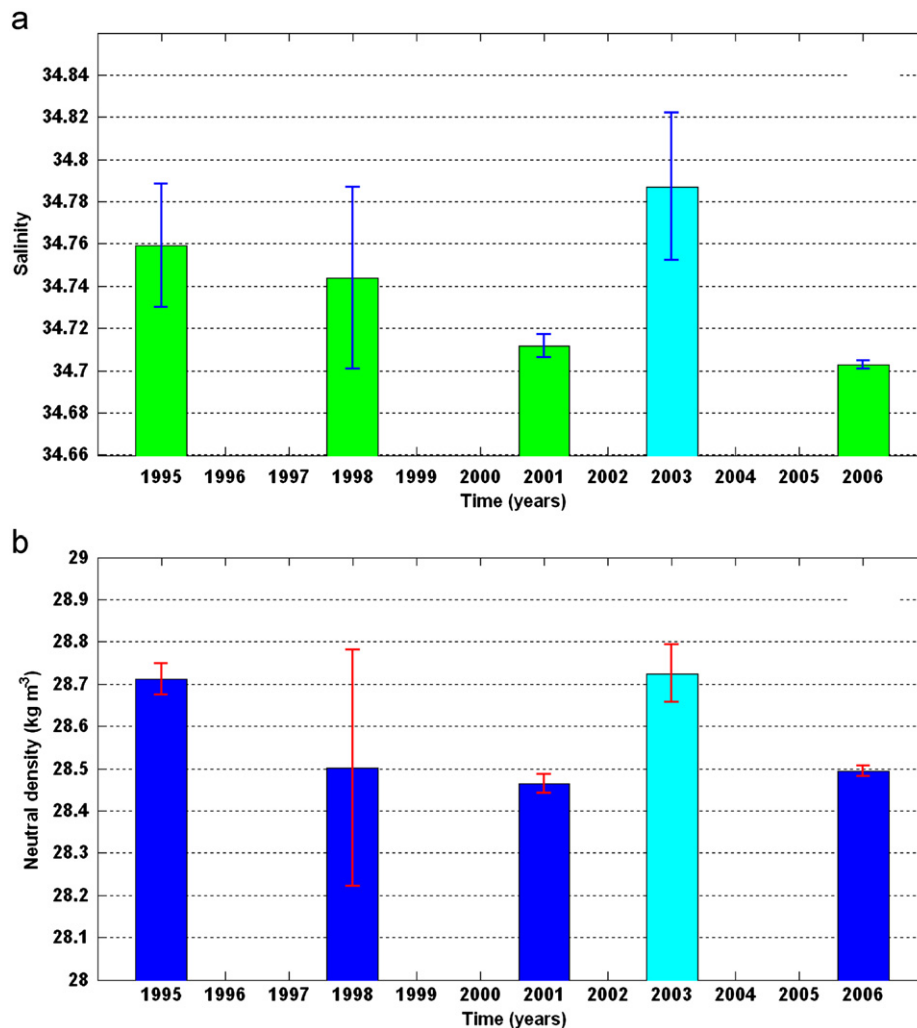


Fig. 7. Averaged values of HSSW ($S > 34.7$) in the bottom layer at the Drygalski Trough of (a) salinity S and (b) neutral density γ^n (kg m $^{-3}$). The anomalous results for the 2003 year are in different color; see text for details. (For interpretation of the references to color in this figure, the reader is referred to the web version of this article.)

anomalous salinity and density values in 2003 (Fig. 7, cyan bars), as also reported by Gordon et al. (2009a); in Section 5 we discuss this anomaly in terms of local forcing due to the temporary presence of a large, tabular grounded iceberg and changes in HSSW production in the TNB Polynya.

4.3.2. Moored time series

We compare the thermohaline data measured by the moored sensors located on the outer continental shelf (locations shown in Fig. 1) with results from analyses of the CTD data, focusing on mooring G (2003–2006) in the DT and mooring H1 (1995–2006, with several gaps) in the GCT. Moorings G and H1 were located ~50 and ~100 km, respectively, from the shelf break to measure the thermohaline characteristics of the shelf water approaching the shelf break before mixing with CDW/MCDW. Whereas the CTD data described in the previous section necessarily represent the thermohaline conditions only during the summer seasons when the CLIMA cruises took place, mooring data provide information throughout the year.

The deeper instrument of mooring G was about 10 m above the bottom; the two year long record (2004–2006) of S at this sensor is shown in Fig. 8. Salinity of the benthic layer fluctuates significantly with different time scales from diurnal to seasonal. The higher salinity values indicate a benthic layer occupied by HSSW (Budillon et al., 2000a, 2000b), while the fresher values indicate intrusions of MCDW southward into the DT. The MCDW intrusions show variability on a fortnightly cycle, which previous authors have attributed to the influence of spring/neap modulation of tidal currents (Whitworth and Orsi, 2006; Padman et al., 2009). There is no clear seasonal variability in the fortnightly periodicity or minimum salinity of the MCDW intrusions; however, there is a large pulse of very fresh ($S \approx 34.57$) water in late December 2004.

The low-passed time series of S for the same sensor data shows strong seasonal variability (Fig. 8), with higher values in March–April and minima in October. There is also significant interannual variability, with much higher salinities in 2004. If we compare the mooring results with Fig. 7a based on CTD, the high salinity in early 2004 looks like the 2003 anomaly identified in CTD data (see Section 4.3.1).

The CLIMA cruises were usually carried out during January–February; i.e., roughly corresponding to the period of maximum HSSW presence and maximum high-frequency variability of benthic salinity in the northern Drygalski Basin (Fig. 8). The associated sampling bias must be considered when estimating thermohaline trends from cruise data.

At mooring H1, ~100 km south of the shelf break in the GCT, the benthic layer is primarily composed of ISW (temperature below the surface freezing point) and HSSW. The former comes from beneath the Ross Ice Shelf (Jacobs et al., 1985; Budillon et al., 2002a, 2002b; Rubino et al., 2003; Smethie and Jacobs, 2005), while the latter comes from the TNB Polynya following the topographic depressions of the western Ross Sea (Jacobs et al., 1985; Budillon et al., 2003). At mooring H1, where the salinity contrast between MCDW and SW is much lower than in the DT (see Fig. 4), temperature rather than salinity provides the clearest discrimination between shelf waters and the CDW/MCDW from the adjacent deep ocean. The potential temperature at the bottom (θ_b) fluctuates significantly at diurnal, fortnightly and seasonal scales (Fig. 9). The low-passed values of θ_b indicate seasonal variability with higher temperatures in May/June. There was an abrupt change during the austral summer 2001/2002 when θ_b increased from -1.92 °C to -1.90 °C over ~6 months, after which it remained at the higher level. We do not yet understand the cause of this relatively rapid increase in θ_b .

The benthic shelf water in the GCT became warmer and fresher from 1995 to 2006. The frequency plot of Fig. 10 reveals a decrease of the maximum salinity, from 34.76 in 1998 to 34.72 in 2006. At the same time, the most common salinity values recorded in the benthic layer declined from 34.75 in 1998 to 34.71 in 2005. Temperature values below the surface freezing point (≈ -1.93 °C, Fig. 11) reveal the presence of ISW in the benthic layer; ISW was also observed in CTD data from cruises in 1995 and 1998. After 1998, the coldest water in the benthic layer was ~ -1.95 °C (-1.92 °C in 2002).

The frequency plots of Figs. 10 and 11 clearly indicate a continuous presence of HSSW in the benthic layer (high salinity and relatively high temperature) in the GCT, and progressive warming of the benthic layer, during the period discussed here. The presence of HSSW in the GCT is strongly linked with the polynya processes in the TNB (Budillon et al., 2003) and, during the years 1995–2006, HSSW in the TNB Polynya (where is formed) experienced both a freshening and an increase in the transport (see Fusco et al. (2009); their Figs. 5 and 6). If the warming of the benthic layer at mooring H1 in the GCT was due to greater vertical mixing of ISW with LSSW in the intermediate layer, we would expect the bottom layer salinity minimum to change as well. Since it does not do so, we infer a substantial decoupling between LSSW and HSSW in this area. We therefore hypothesize that the warming of the benthic layer in the GCT is related to the change in the properties of HSSW being delivered from the TNB Polynya.

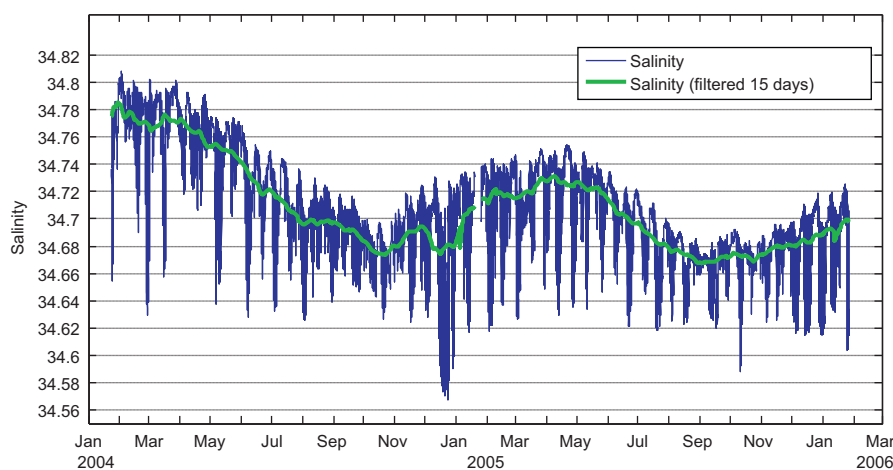


Fig. 8. Time series of salinity S in the benthic layer (about 15 m above the sea bottom) at mooring G in the northern Drygalski Trough (see Fig. 1 for location): hourly (thin line) and low-pass filtered (bold line, cutoff of 15 days) data shown.

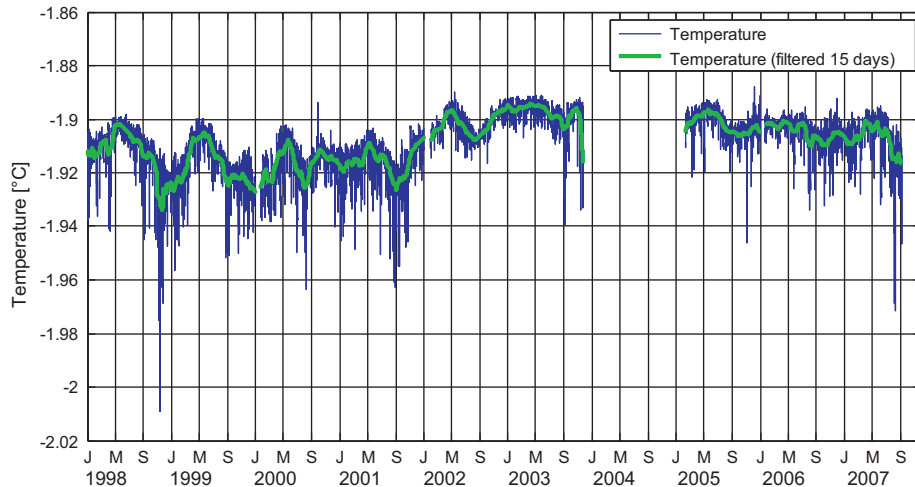


Fig. 9. Time series of potential temperature θ in the benthic layer (about 20 m above the sea bottom) at mooring H1 in the northern Glomar-Challenger Trough (see Fig. 1 for location); hourly (thin line) and low-pass filtered (bold line, cutoff of 15 days) data shown.

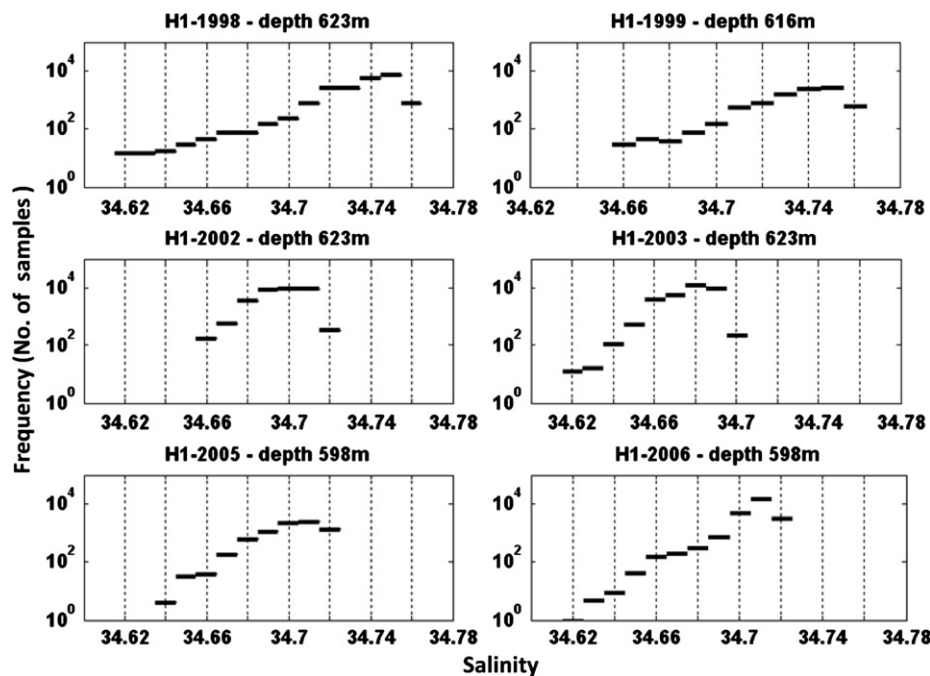


Fig. 10. Histograms of the frequency of salinity S (in 0.01 intervals) from the deepest current meter at mooring H1 (northern Glomar-Challenger Trough) for one-year time intervals from 1998 to 2006.

4.4. Gravity currents on the continental slope at the Glomar-Challenger Trough

Mooring H3 was deployed on January 31, 2005 at the continental slope outside the GCT at the depth of 1216 m just east of the dateline at $\sim 75^\circ\text{S}$ (see Fig. 1 for location), along a possible path followed by the cold benthic outflow (see Fig. 6). The cross-slope CTD/LADCP section performed in this area (Fig. 6) shows the presence of a cold and oxygenated layer of dense shelf water flowing north-westward. Two Aanderaa RCM7 current meters acquired data at 1157 and 1206 m depth (59 and 10 m, respectively, above the bottom). Both instruments often recorded the SW outflow (Fig. 12). Typically, SW was observed when the water speed exceeded 0.5 m s^{-1} towards the north or northwest. These data are consistent with the ISW flowing over the shelf, turning westward due to the Coriolis force, and moving along the

isobaths with a significant downslope benthic flux due to buoyancy, friction and other effects such as thermobaricity.

The bottom current meter measured a mean flow of $(u, v) = (-11.7, +42.3) \text{ cm s}^{-1}$, which is roughly parallel to the isobaths. The mean temperature recorded by the Arctic-range sensor was $T = -0.592^\circ\text{C}$. The lowest temperature bottom water corresponds to periods of strong offshore flow while the warm temperatures are found during the phases of slow flow. This behavior is similar to that observed by Padman et al. (2009; their Fig. 13) for a continental slope site near the DT; see, also, Gordon et al. (2004) and Visbeck and Thurnherr (2009).

The upper current meter ($\sim 59 \text{ m}$ from the bottom) measured a mean flow of $(u, v) = (-20.7, +44.2) \text{ cm s}^{-1}$; again, roughly parallel to local isobaths. The mean temperature here was $T = -0.337^\circ\text{C}$ for the standard sensor. The cold (warm) temperatures always occur when the v component (approximately

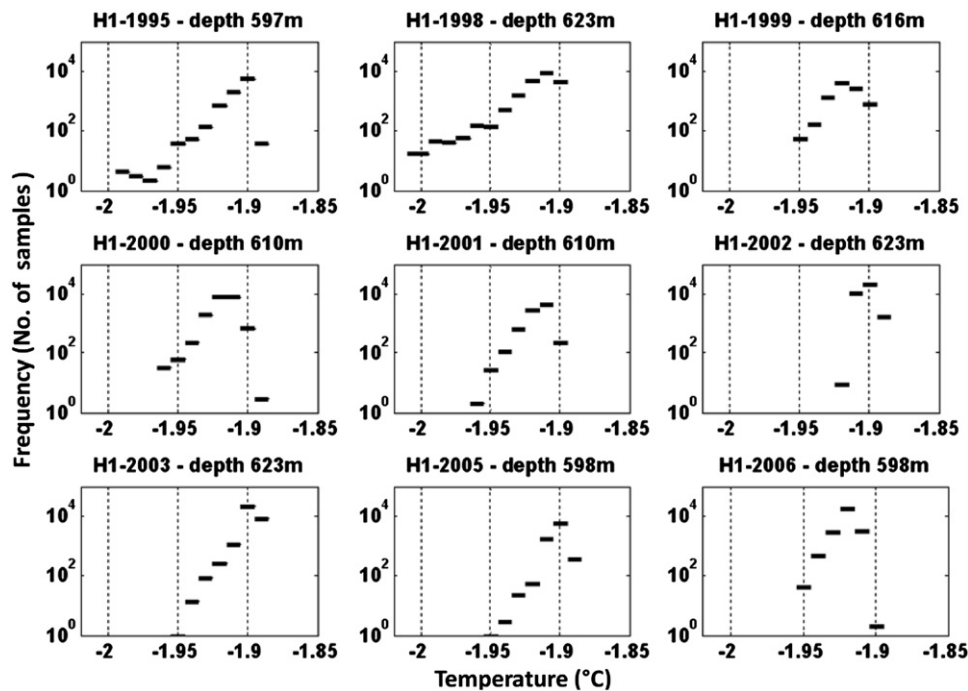


Fig. 11. Histograms of the frequency of temperature ($^{\circ}\text{C}$) (in 0.01°C bins) from the deepest current meter at mooring H1 (northern Glomar-Challenger Trough) for one-year time intervals from 1995 to 2006.

perpendicular to the isobaths) reaches the maximum (minimum) values. However, there is little correlation between T and the u component, flowing roughly parallel to the isobaths. The analysis of the time series clarifies that, at the mooring location, the 1200 m isobath can be crossed by the undiluted cold water coming from the shelf only when the v component exceeds $\sim 0.6\text{ m s}^{-1}$.

Cold events at mooring H3 comprise a relatively small fraction of the total data set. Observations of $\theta_b < -1.8^{\circ}\text{C}$ comprise only $\sim 7\%$ of the total record, while for colder threshold values of -1.85°C and -1.92°C , the fractions are 2.9% and 0.8%, respectively.

We analyzed the velocity time series from the bottom current meter for tidal constituents using the T_tide Matlab[®] routines (Pawlowicz et al., 2002), which are based on the methods described by Foreman (1978). These analyses underline the importance of the tide in this area; Table 3 gives the results for the most important constituents. Diurnal tidal constituents K_1 and O_1 dominate the tidal current signals, consistent with previous studies for the Ross Sea (Erofeeva et al., 2005; Robertson, 2005; Johnson and van Woert, 2006).

A qualitative correlation between tides and the presence of ISW plumes in the benthic layer at mooring H3 can be seen in Fig. 13. The time series of the fitted v component (roughly cross-slope) of the tidal signal (Fig. 13b) shows the expected spring/neap cycle. The residual current (Fig. 13c), determined by removing the fitted tidal signal from the measured data, still includes periodic signals at tidal frequencies; this signal may indicate nonlinearities in the tidal currents, associated with interactions with the mean flow and gravity flow “events”; see, also, Padman et al. (2009). The time series of θ_b (Fig. 13d) is dominated by tidal frequencies. A rapid decrease in θ_b is always related to a sudden increase in v , consistent with Fig. 12. Benthic temperature is correlated with the phase of the spring/neap modulation. During neap tides, θ_b is usually below 0°C , variability is relatively low, and the low-passed temperature is also low ($\sim -1^{\circ}\text{C}$). During spring tides, variability of θ_b is higher and low-passed temperature is warmer, approaching 0°C . Temperature sometimes exceeded

$+0.5^{\circ}\text{C}$ during spring tides (cf. Fig. 11 in Muench et al., 2009a) but was also frequently $< -1.9^{\circ}\text{C}$ as almost pure SW was advected past mooring H3 by offshore tidal flows.

Without additional information from above and below mooring H3 on the slope, we cannot tell whether these changes represent significant temporal variability in outflow properties or simply a shift in the depth of the dense outflow as it flows westwards along the continental slope past mooring H3. However, by comparison with the modeling studies of Padman et al. (2009) and Wang et al. (2010), we assume that tidal modulation of mixing and advection at the slope near the GCT plays a similar role to that observed at the DT, leading to a fortnightly modulation of AABW volume flux and hydrographic properties.

To explore the relationship in time-frequency space of such energetic cold episodes, we used wavelet analysis (Section 3.4). To highlight the cold events at periods longer than the tidal frequency we analyzed the residual current (see Fig. 13c). Despite the detiding prior to wavelet analysis, energetic benthic flow events occur at the fundamental tidal period (about 24 h), modulated by the 14-day spring/neap cycle (Fig. 14). Less regular, energetic signals are also found in the band between 1.5 and 2.4 days (about 32–64 h) and at longer time scales (4–5 days, or $\sim 100\text{ h}$). These time scales are reminiscent of variability in the Filchner Trough outflow (Darelius et al., 2009), which has been attributed to barotropic eddies associated with the density outflow (Wang et al., 2009).

In the period between early June and mid-July 2005, a dominant period of about four days is evident. This period of the year roughly corresponds to the beginning of the colder phases that we detected each year at mooring H1 (about 100 km southward over the shelf) during 2000–2003 (Fig. 9). Variability at periods greater than five days is not very well resolved by this wavelet analysis; however, we can identify the presence of energetic low-frequency peaks at the beginning of March, late July and early August, at the beginning of September, and at the beginning of October.

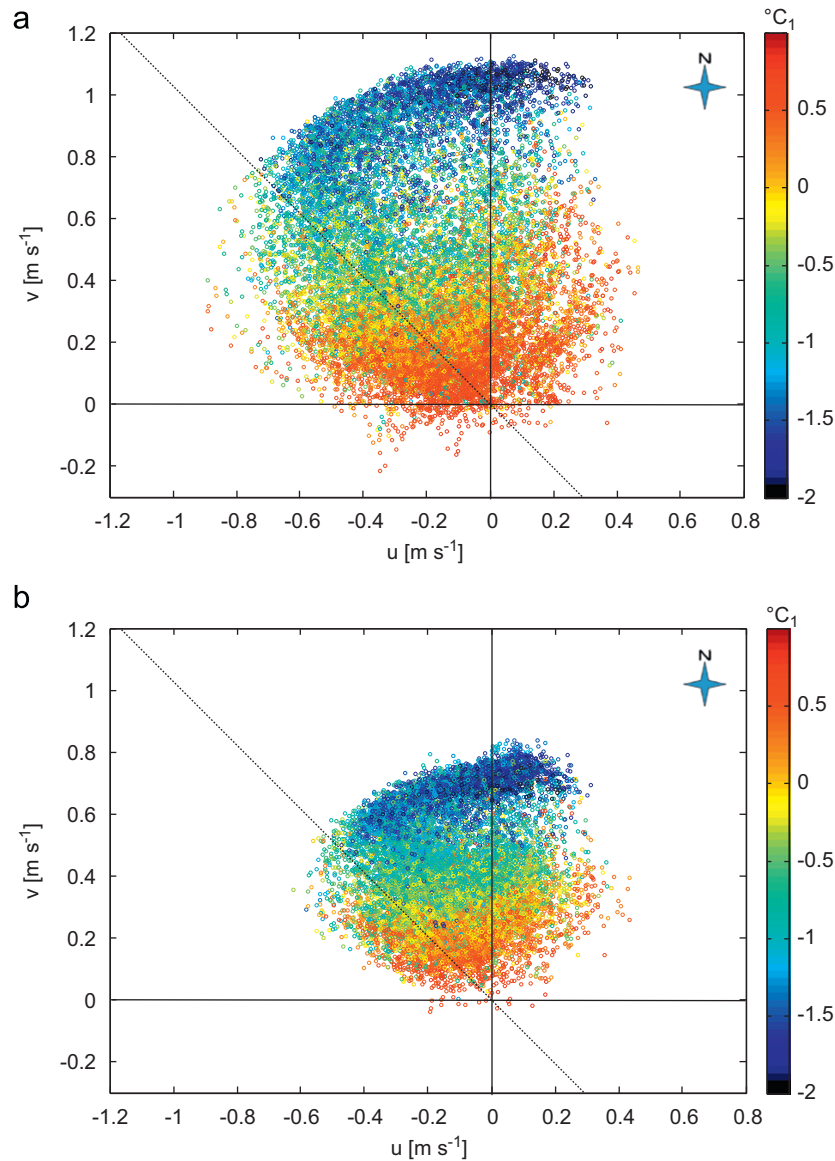


Fig. 12. Scatter plot of hourly u vs. v (m s^{-1}) for mooring H3, with temperature ($^{\circ}\text{C}$) color coded: (a) current meter at 1157 m depth (59 m above the bottom); (b) current meter close to the bottom (10 m above the bottom, 1206 m depth). The dashed diagonal line represents the approximate direction of local isobaths. (For interpretation of the references to color in this figure, the reader is referred to the web version of this article.)

Table 3

Coefficients for most energetic tidal harmonics for the bottom current meter (1392 m depth, 8 m above the bottom) at mooring H3 (75.04243°S , $183.51665^{\circ}\text{E}$) on the continental slope north of Glomar-Challenger Trough, obtained with “T_Tide” Matlab toolbox (Pawlowicz et al., 2002). For each harmonic, columns show: frequency ω (cycles per hour); major axis and error (U_{maj} and ε_{maj} ; m s^{-1}); minor axis and error (U_{min} and ε_{min} ; m s^{-1}); ellipse inclination (inc), ellipse phase G_o and phase error ε_{pha} ; and signal-to-noise ratio (snr). MF is a fortnightly (long-period) tide; O_1 , P_1 and K_1 are diurnal harmonics; and K_2 is the only energetic semidiurnal harmonic.

Tide	ω	U_{maj}	ε_{maj}	U_{min}	ε_{min}	inc	einc	G_o	ε_{pha}	snr
MF	0.00305	0.038	0.003	0.013	0	98.21	4.42	47.82	5.48	130
O_1	0.038731	0.066	0.002	0.036	0	23.37	3.78	352.81	3.73	860
P_1	0.041553	0.05	0.002	0.042	0	21.57	15.24	290.04	14.13	480
K_1	0.041781	0.166	0.002	0.141	0	179.32	4.16	94.41	3.75	10,000
K_2	0.083562	0.025	0.002	0.017	0	117.01	11.07	215.05	11.67	130

5. Discussion

The results described in the previous section show large spatial and temporal variability of the characteristics of the ASF, shelf water masses, and the outflows leading to AABW input to the global ocean along the continental margin of the Ross Sea. In

this section we relate this variability near the shelf break to what is known about larger-scale changes in the Ross Sea.

The ASF is a slightly porous dynamic barrier between the warm intermediate water (CDW) of the deep ocean and the colder, denser water found on the continental shelf. As we have shown, the ASF never moves inshore of the shelf break in the GCT,

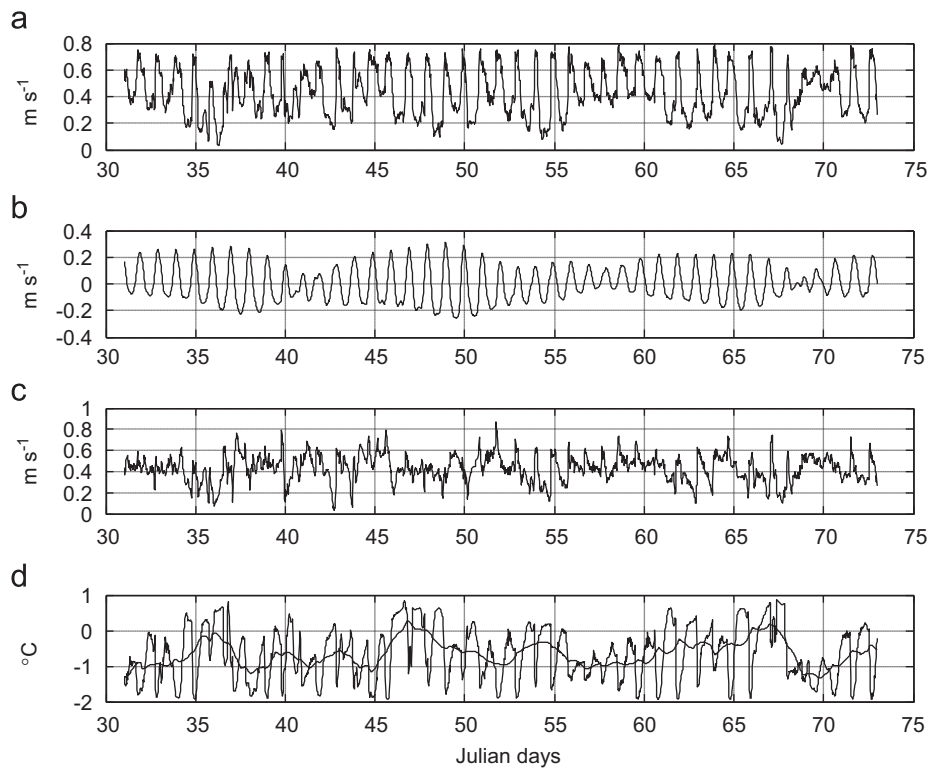


Fig. 13. (a) Six-week subset of north (approximately cross-slope) component of current (v ; m s^{-1}) at mooring H3 bottom current meter (1206 m depth, 10 m above the bottom). (b) Tidal component of v , determined with T-tide (see text). (c) Residual component of v , determined by removing fitted tidal current from measured current. (d) Hourly measured temperature ($^{\circ}\text{C}$) (thin line) and low-pass filtered (bold line) with a cutoff of 1 day.

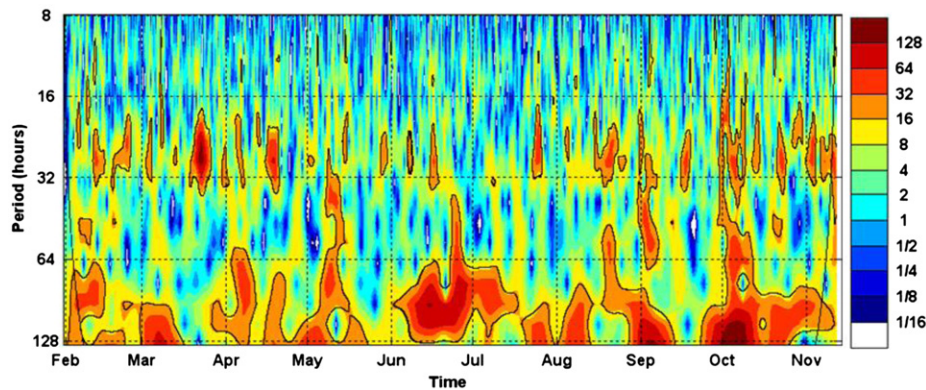


Fig. 14. Wavelet power spectrum (m^2/s^2) for the residual v component of the bottom current meter of mooring H3 (1206 m depth, 10 m above the bottom); i.e., time series shown in Fig. 13c.

but is frequently found south of the shelf break in the DT. This difference in behavior appears to be related to the strength of cross-slope tidal currents and the steepness of the continental slope; as Muench et al. (2009a) and Padman et al. (2009) showed, cross-slope advection of the ASF near the DT can be up to ~ 20 km, sufficient to carry water parcels between the outer shelf and the central slope near the 1500 m isobath. Weaker tidal currents and a less steep continental slope near GCT (see Padman et al., 2009; their Fig. 3) reduce the impact of tidal advection in that region. The weaker tides near the GCT also reduce the mixing of the benthic layer of dense shelf water with adjacent water masses (Whitworth and Orsi, 2006; Padman et al., 2009). Cold shelf water (SW) flowing north along the GCT is, therefore, relatively unmodified by the time it reaches the shelf break, so that almost pure SW is fairly frequently found over the continental slope. This also means that the initial mixing between

shelf water (mostly ISW) and CDW/MCDW required for AABW formation occurs below the depth of the shelf break where the CDW is cooler (~ 0.6 $^{\circ}\text{C}$) than at the depth of θ_{max} (~ 400 m, where $\theta \approx 1.2$ $^{\circ}\text{C}$; see Fig. 6). In contrast, tidal advection bringing the ASF inshore of the shelf break near the DT (see Fig. 5) allows mixing to occur directly between the HSSW and the warmest CDW (Fig. 4), before the dense shelf water begins to descend the slope.

As Budillon et al. (2000a, 2000b) noted from their analyses of CTD data collected between the ASF and the Italian base at Terra Nova Bay, the intrusion of CDW and MCDW can reach $\sim 74^{\circ}\text{S}$ following the eastern flank of the DT. Rusciano et al. (2008) found, from mooring data from 1995 to 2006, evidence of MCDW within the TNB Polynya itself. That is, tidal advection of the ASF across the shelf break at the DT, followed by mixing and wind-forced advection, appears to support direct ventilation of the primary

HSSW source region (TNB) by MCDW. This two-way, direct connection between TNB and the deep ocean north of DT implies potential for rapid response of TNB hydrography to changes in the larger-scale circulation of the Ross Gyre (Jacobs et al., 2002), and of the global meridional overturning circulation to atmospheric and other changes in TNB. For example, if the Drygalski Ice Tongue that forms a sea ice “dam” on the southern edge of the TNB Polynya was to break off, we would expect rapid changes in HSSW formation to propagate rapidly throughout the Ross Sea. Furthermore, since HSSW from TNB is the primary source water circulating under Ross Ice Shelf (RIS), these interactions connect ISW production (from basal melt under the RIS) to the deep ocean north of the DT.

The dominance of tides in the across-slope velocity at the shelf break and upper continental slope has implications for sampling the ASF. During CLIMA cruises, transects across the slope typically took several hours to complete; e.g., in creating Fig. 6, cast #64 near the 1800 m isobath was completed 7 h later than cast #59 over the outer shelf. In this time, tidal advection can move the ASF several km across-slope (see Muench et al., 2009a; their Fig. 11) at spring tides, so that the structure of the ASF mapped by the CTD measurements could be biased by tidal advection. However, since the tidal currents are significantly weaker at the GCT, we expect less aliasing of tidal advection even at spring tides. Indeed, we obtained similar results from several transects collected perpendicular to the slope near the GCT at different times and different tidal phases (not shown here).

While differences in cross-slope tidal advection along the shelf break appear to be important to ventilating the continental slope with warm CDW/MCDW, other mechanisms are also potentially significant. Dinniman and Klinck (2004) used a numerical model of CDW intrusions to show that CDW tends to cross the shelf break in places where shelf break curvature is such that the inertia of the along-slope current (ASF) tends to carry water upslope. Both the strength of the current and the topographic curvature play a role in determining the efficiency of this mechanism. The onshore flux of CDW-derived heat in this manner is modulated in time (Dinniman and Klinck, 2004) by instabilities of the ASF and changes in the local and regional wind stress fields. Unfortunately, wind stress variability is poorly known over Antarctic coastal waters and the Southern Ocean because of a paucity of direct observations for assimilation into global and regional atmospheric models.

As we noted earlier when discussing the direct connections between the deep water north of the DT and the TNB Polynya (and, ultimately, to ISW production), the ability to rapidly propagate an anomaly through the entire shelf system implies that the dense water and sea ice production over the continental shelf can change rapidly in response to variations in atmospheric and oceanic variability north of the shelf break. Furthermore, rapid changes in these processes over the shelf can be imposed quickly on the world ocean through variations in the dense water outflow fluxes and hydrographic properties.

Evidence for the ability of the Ross Sea system to respond rapidly to changes comes from our measurements of variability in the HSSW in the northern DT and ISW in the northern GCT (Section 4.3, and Figs. 7–11). These data show a general freshening of the HSSW in the northern DT of about 0.06 (Fig. 7), generally consistent with an earlier study of trends in water mass properties in the Ross Sea (Jacobs et al., 2002). This freshening trend was, however, interrupted by a very rapid increase in HSSW salinity between 2001 and 2003 (Fig. 7) and the subsequent rapid drop of ~ 0.08 by 2006. Gordon et al. (2009a) argued that the increased HSSW salinity in 2003 was associated with the presence of the large grounded iceberg C-19 over the Mawson–Crary Bank, through the effects of the temporary “island” modifying

ocean and sea ice circulation in this region. (See, also, a modeling study by Dinniman et al. 2007 of the effect of grounded icebergs in the Ross Sea.) However, Fusco et al. (2009) also reported a large production of HSSW during 2003–2004 in the TNB Polynya, regarded as the most important formation area for HSSW in the Ross Sea. Considering the relatively short distance between this formation area and Cape Adare (about 450 km) and a mean velocity of 0.025 m s^{-1} (inferred by comparing the timing of salinity maxima at TNB and northern DT), the anomaly in salinity formed in TNB would reach the shelf break in a few months. This speculation is supported by the analysis of the CFC contents in the samples collected between the TNB Polynya and the shelf break at the DT; the results showed that the HSSW takes less than one year to reach the shelf break at the DT (Rivaro et al., 2003). Regardless of the explanation for the change in HSSW characteristics in the northern DT, it is clear that perturbations in one part of the Ross Sea can be rapidly transmitted to other regions.

The observation, from mooring H3, that ISW can be found intermittently near the 1200 m isobath near GCT (Section 4.4; Figs. 4b, 12 and 13) implies that some process can advect pure shelf water down from the shelf break without appreciable mixing. Two dynamical reasons have been previously proposed to explain similar observations in the Filchner Trough outflow in the southern Weddell Sea (Foldvik et al., 2004; Darelus et al., 2009). The thermobaric effect, which is the increase in *in situ* density with increasing pressure (compressibility), is larger in cold plumes than in the adjacent waters. Thus, as the plume descends, the density step at the top of the plume increases, suppressing mixing between the plume and the overlying warmer water (Killworth, 1977). This effect is clearly revealed in our case by comparing the θ/S diagram of Fig. 4b, where the density contrast between the CDW and the bulk of the ISW increases with depth. Second, supercritical flows lead to a strong reduction in mixing behind irregularities in the bottom topography (Long, 1954). This process allows plumes of dense water to reach great depths with little mixing and much reduced friction. We estimate the phase speed at the ISW/CDW interface as

$$c_p = (g'H)^{1/2}$$

where g' is the reduced gravity ($g' = g\Delta\rho/\rho$) and H is the thickness of the plume. Flows with speeds $> c_p$ are supercritical. Considering the typical thickness ($H=200 \text{ m}$) of the benthic plume based on the CTD measurements performed in this area (Fig. 6), we obtain $c_p \approx 0.4 \text{ m s}^{-1}$. From the velocity time series collected at mooring H3, the plume flow is often supercritical ($|\mathbf{u}| > c_p$) so that mixing is negligible; the dense plume of ISW may, therefore, reach considerable depths with substantially undiluted water.

The overflow of shelf waters at the continental slope may initially reach supercritical speed as a result of flow convergence due to vorticity conservation as the flow experiences converging isobaths, and/or by the downslope buoyancy forcing aided by thermobaricity (Killworth, 1977). Flow convergence should, however, accelerate the entire water column without discriminating between water masses; that is, it will not increase the velocity step at the top of the plume. In contrast, thermobaricity will act most strongly on the cold plumes. The role of thermobaricity is suggested in our data by the strong correlation between high downslope speed and very cold bottom water (Figs. 12 and 13).

The sensitivity of outflow mixing to the properties of both the shelf water and the “ambient” pool of CDW over the continental slope suggests that the resultant AABW properties will change significantly through fairly minor perturbations in the small band of ocean either side of the shelf break. For example, a change in wind stress that shifts the mean location of the ASF across the slope will change the hydrographic characteristics adjacent to the dense outflow, thus affecting the impact of thermobaricity.

Changes in shelf water characteristics, whether through changes in the rate of shelf water production or increased mixing, will influence the thickness and density anomaly of the outflow reaching the continental slope. These will modify the velocity step at which the transition to supercritical flow occurs and, as for thermobaricity, change the potential for dilution of the outflow by entrainment of the ambient water along the outflow path.

6. Conclusions

Correctly representing the exchange of ocean heat and fresh water across the Ross Sea continental slope and shelf break is essential to accurately model the contribution of the Ross Sea to total Antarctic Bottom Water (AABW) production. Changes in the inflow of oceanic heat to the Ross Sea continental shelf will also affect the net production of sea ice in the Ross Sea, and the stability of the Ross Ice Shelf through changes in basal melt rate and calving. The latter have potential impacts on the off-continent flow of the buttressed ice streams and glaciers and, therefore, influence global sea level.

Our measurements of hydrography and velocity collected by CTD/LADCP profiling and from oceanographic moorings during five Italian CLIMA expeditions carried out between 1995 and 2006 provide the first decade-length time series of variability near the shelf break in the central and western Ross Sea. The data provide information about regional differences in the structure of the Antarctic Slope Front (ASF), interannual variability in the properties of the principal shelf water masses, and temporal variability in the ASF and the AABW outflow on time scales from tidal (< 1 day) to interannual.

Comparison of hydrographic properties on the outer shelf at the northern ends of the Drygalski and Glomar-Challenger Troughs (DT and GCT, respectively) demonstrates that: (a) the primary dense source water at the DT is HSSW, while ISW dominates in the GCT; (b) the properties of each shelf water type changed significantly during the decade; (c) the ASF position is much more stable at the GCT than at the DT; and (d) significant mixing occurs between the CDW and SW over the outer shelf of the DT, but not over the outer shelf of the GCT.

Time series of hydrographic properties at moorings G and H1, respectively, deployed ~50 and ~100 km south of the shelf break in the western (DT) and central (GCT) sectors, showed clear seasonal variability in the thermohaline characteristics of both HSSW and ISW. The salinity of HSSW flowing toward the shelf break in the DT is highest at the end of the austral summer (March/April) and lowest in October/November. The ISW in the GCT was coldest in August–October and warmest in March/April (with a few exceptions). The timing of these extrema presumably represent the combination of the annual cycle of forcing (HSSW production in Terra Nova Bay Polynya and basal melting under the Ross Ice Shelf) and advection times for these water masses to arrive at the northern DT and GCT.

The ASF is frequently found well inshore of the shelf break at the DT due to advection by energetic spring tides (Padman et al., 2009). This allows CDW to mix directly with HSSW over the outer shelf in a region of strong tidal mixing (Whitworth and Orsi, 2006; Padman et al., 2009) so that, in general, the dense water reaching the shelf break is significantly warmer and less dense than further south along the DT. (Occasional pulses of cold, dense water are found, however, over the continental slope north of DT under favorable tidal conditions; see Gordon et al., 2004 and Muench et al., 2009a.) In contrast, the shelf water reaching the shelf break at the GCT is fairly unmixed cold, dense water so that most mixing leading to AABW formation occurs on the continental slope. This observation implies that production of AABW near

the DT involves mixing with warmer and saltier CDW than at the GCT, since the initial mixing occurs higher in the water column closer to the depth of $\theta_{\max}(\text{CDW})$, ~400 m. As a result, the distinct processes and different shelf water sources produce different types of AABW in the western and central sectors, with the former being much warmer, more saline and less dense than the latter.

Outflows of dense shelf water can reach depths greater than 1500 m substantially unmixed, most frequently near the GCT but occasionally also near the DT. The events near the DT were not seen in our data sets but were observed during AnSlope (Gordon et al., 2004, 2009a; Padman et al., 2009). The plume of dense water at this depth can flow at speeds approaching 1 m s^{-1} , probably aided by thermobaricity, and implying that the flow is occasionally supercritical; compare with observations from the Filchner Trough outflow in the southern Weddell Sea (Foldvik et al., 2004; Darelius et al., 2009). Analyses of time series collected at mooring H3 positioned near the 1200 m isobath on the continental slope just west of the GCT allowed us to characterize the benthic plumes of ISW. Tides modulate the dense water outflow, with energetic plumes of unmodified ISW being more frequent during the spring tides (cf. Gordon et al., 2004); however, the mean temperature of the outflow is lower during neap tides (Fig. 13) due to fewer occurrences of CDW/MCDW. That is, the ASF generally remains offshore of mooring H3 except when spring tides advect the ASF into shallower water. Using wavelet analysis we also detected several intermittent episodes of energetic currents with characteristic time scales of 32–64 h, and 4–5 days. These time scales are reminiscent of recent work on the Filchner Trough outflow in the Weddell Sea (Darelius et al., 2009; Wang et al., 2009), where the time scales appear to be set by the characteristics of barotropic eddies associated with the density outflow.

The thermohaline characteristics of both shelf water types, ISW in the GCT and HSSW in the DT, changed during the decade 1995–2006. In the central Ross Sea (GCT) the ISW freshened by ~0.04 during 1998–2006 and warmed about 0.04 °C between 1995 and 2006, with a rapid increase of the temperature during the austral summer 2001/02 (Fig. 10). The HSSW at the western shelf break (DT) freshened by ~0.06 from 1995 to 2006 (Fig. 7), with consequences for the resulting AABW salinity and density (e.g., Rintoul, 2007). The 2003 data collected in the western sector of the Ross Sea recorded a saltier anomaly in the deep layers (Figs. 7 and 8). As suggested by Gordon et al. (2009a), the presence of the mega-iceberg C-19 may have had a significant impact on the local circulation by changing the apparent regional topography (see also, Dinniman et al., 2007). Alternatively, larger production of HSSW in the same year in the TNB Polynya produced by strong air–sea heat fluxes at that time (Fusco et al., 2009) may have significantly increased the salinity of the HSSW flowing north to the western shelf break along the DT.

This study highlights the importance of long-term sampling of hydrography and currents in a region whose contributions to AABW formation, sea ice production and fresh water flux to the global ocean could change quite rapidly through the interaction of several mechanisms operating on a wide range of time and space scales. We still have a poor understanding of how the heat from the offshore CDW crosses the ASF to the continental shelf and further south to the ice shelf. Atmospherically-forced ocean models reproduce some of this flux (Dinniman et al., 2003, 2007) but rely on atmospheric models that are poorly constrained by *in situ* data. Models are also sensitive to bathymetry, which is not well known for many sectors of the outer continental shelf of the Ross Sea. At long time scales, we do not yet have the measurements required to determine the effects of large-scale iceberg calving from the Ross Ice Shelf front, or the potential influence of the future loss of the

Drygalski Ice Tongue that forms the southern boundary of the Terra Nova Bay Polynya. The ultimate volume flux and hydrographic properties of AABW from the Ross Sea sector also depends on small-scale processes, including tidal advection and mixing, generation of barotropic eddies in the dense water outflows and interaction of the outflow and the ASF with small-scale bathymetric features such as seabed channels (Muench et al., 2009b) and sharp bends in the continental slope (Padman et al., 2009; Wang et al., 2010). Improving our understanding of the entire Ross Sea physical system and its interaction with the global ocean requires further data acquisition and related modeling aimed at these processes and their interactions.

Acknowledgments

We thank Bruce Huber (LDEO—USA) for valuable guidance on installing the LADCP system and Martin Visbeck (IFM-GEOMAR—Germany) for providing the LADCP processing software (<http://ladcp.ldeo.columbia.edu/ladcp/>). Arturo de Alteris, Massimo De Stefano and Giovanni Zambardino provided excellent support during the field operations.

Logistical and financial support for the CLIMA IV project was provided by the Italian National Program for Antarctic Research (PNRA). LP was funded by the U.S. National Science Foundation Antarctic Sciences program, grant ANT-0440656. This is ESR Contribution number 139.

We appreciate the detailed, constructive comments from two anonymous reviewers.

References

- Ainley, D.G., Jacobs, S.S., 1981. Sea-bird affinities for ocean and ice boundaries in the Antarctic. *Deep-Sea Research* 28A (10), 1173–1185.
- Aoki, S., Rintoul, S., Ushio, S., Watanabe, S., Bindoff, N.L., 2005. Freshening of the Adélie Land Bottom Water near 140°E. *Geophysical Research Letters* 32, L23601. doi:10.1029/2005GL024246, 2005.
- Baines, P.G., Condie, S., 1998. Observations and modeling of Antarctic downslope flows: a review. In: Jacobs, S., Weiss, R. (Eds.), *Ice and Atmosphere: Interaction of the Antarctic Continental Margin*, 75. American Geophysical Union, pp. 29–49.
- Bergamasco, A., Defendi, V., Meloni, R., 2002a. Some dynamics of water outflow from beneath the Ross Ice Shelf during 1995–1996. *Antarctic Science* 14, 74–82.
- Bergamasco, A., Defendi, V., Zambianchi, E., Spezie, G., 2002b. Evidence of dense water overflow on the Ross Sea shelf-break. *Antarctic Science* 14 (3), 271–277.
- Bergamasco, A., Defendi, V., Budillon, G., Spezie, G., 2004. Down flow observations near Cape Adare shelf-break. *Antarctic Science* 16 (2), 199–204.
- Budillon, G., Spezie, G., 2000. Thermohaline structure and variability in the Terra Nova Bay Polynya, Ross Sea. *Antarctic Science* 12 (4), 493–508.
- Budillon, G., 2007. The Ross Sea. In: Riffenburgh, Beau (Ed.), *Encyclopedia of the Antarctic*, 2 vols.; 2007.
- Budillon, G., Pacciaroni, M., Cozzi, S., Rivaro, P., Catalano, G., Ianni, C., Cantoni, C., 2003. An optimum multiparameter mixing analysis of the shelf waters in the Ross Sea. *Antarctic Science* 15 (1), 105–118.
- Budillon, G., Massolo, S., Rivaro, P., Spezie, G., 2002a. Studies of deep water formation and mixing in the Ross Sea using anthropogenic tracers. In: *Proceedings of the second GLOBEC Open Science Meeting Comparative Ecosystem and Climate Change* 15–18.10.2002 (a), Qingdao, PR China.
- Budillon, G., Gremes Cordero, S., Salusti, E., 2002b. On the dense water spreading off the Ross Sea shelf (Southern Ocean). *Journal of Marine Systems* 35, 207–227.
- Budillon, G., Tucci, S., Artegiani, A., Spezie, G., 2000a. Water masses and suspended matter characteristics of the Western Ross Sea. In: Faranda, F.M., Guglielmo, L., Ianora, A. (Eds.), *Ross Sea Ecology*. Springer-Verlag, pp. 63–81 ISBN:3-540-65372-4.
- Budillon, G., Fusco, G., Spezie, G., 2000b. A study of the heat fluxes in the Ross Sea (Antarctica). *Antarctic Science* 12 (2), 243–254.
- Budillon, G., Salusti, E., Tucci, S., 2006. The evolution of density currents and nepheloid bottom layers in the Ross Sea (Antarctica). *Journal of Marine Research* 64 (4), 517–540.
- Burrus, C.S., Gopinath, R.A., Guo, H., 1998. *Introduction to Wavelets and Wavelet Transforms*. A Primer. Prentice Hall, Upper Saddle River, NJ (USA).
- Darelius, E., Smedsrud, L.H., Østerhus, S., Foldvik, A., Gammelsrød, T., 2009. Structure and variability of the Filchner overflow plume. *Tellus* 61A, 446–464.
- Daubechies, I., 1994. Ten lectures on wavelets. CBMS, SIAM 61 (1994), 76.
- Davey, F.J., Nitsche, F., 2005. Bathymetric grid of the Ross Sea, Antarctica. Electronic format: <<ftp://ftp.ldeo.columbia.edu/pub/fnitsche/RossSeaBathymetry/>>.
- Dinniman, M.S., Klinck, J.M., 2004. A model study of circulation and cross-shelf exchange on the west Antarctic Peninsula continental shelf. *Deep-Sea Research II* 51, 2003–2022.
- Dinniman, M.S., Klinck, J.M., Smith Jr., W.O., 2003. Cross-shelf exchange in a model of the Ross Sea circulation and biogeochemistry. *Deep-Sea Research II* 50, 3103–3120.
- Dinniman, M.S., Klinck, J.M., Smith Jr., W.O., 2007. Influence of sea ice cover and icebergs on circulation and water mass formation in a numerical circulation model of the Ross Sea, Antarctica. *Journal of Geophysical Research* 112, C11013.
- Erofeeva, S.Y., Padman, L., Egbert, G., 2005. Assimilation of ship-mounted ADCP data for barotropic tides: application to the Ross Sea. *Journal of Atmospheric and Oceanic Technology* 22, 721–734.
- Fahrbach, E., Harms, S., Rohardt, G., Schröder, M., Woodgate, R.A., 2001. Flow of bottom water in the northwestern Weddell Sea. *Journal of Geophysical Research* 106 (C2), 2761–2778.
- Foldvik, A., Gammelsrød, T., Østerhus, S., Fahrbach, E., Rohardt, G., Schröder, M., Nicholls, K.W., Padman, L., Woodgate, R.A., 2004. Ice shelf water overflow and bottom water formation in the southern Weddell Sea. *Journal of Geophysical Research* 109, C02015. doi:10.1029/2003JC002008.
- Foreman, M.G.G., 1978. *Manual for tidal currents analysis and prediction*. Pacific Marine Science Report. 78-6. Institute of Ocean Sciences, Patricia Bay. 57 pp.
- Foufoula-Georgiou, E., Kumar, P., 1995. *Wavelet in Geophysics*. Academic Press 373.
- Fusco, G., Budillon, G., Spezie, G., 2009. Surface heat fluxes and thermohaline variability in the Ross Sea and in Terra Nova Bay polynya. *Continental Shelf Research* 29, 1887–1895.
- Gordon, A.L., 1974. Varieties and variability of Antarctic bottom water. In: *Processus de Formation des Eaux Oceaniques Profondes (en particulier en Mediterranee Occidentale)*. Editions du Centre National de la Recherche Scientifique, Paris, France, No. 215, pp. 33–47.
- Gordon, A.L., Zambianchi, E., Orsi, A., Visbeck, M.C., Giulivi, F., Whitworth III, T., Spezie, G., 2004. Energetic plumes over the Western Ross Sea continental slope. *Geophysical Research Letters* 31, L21302. doi:10.1029/2004GL020785.
- Gordon, A.L., Orsi, A.H., Muench, R.D., Huber, B.A., Zambianchi, E., Visbeck, M., 2009a. Western Ross Sea continental slope gravity currents. *Deep-Sea Research II* 55. In: Gordon, A., Padman, L., Bergamasco, A. (Eds.), *Deep-Sea Research Part II. Southern Ocean Shelf Slope Exchange*. doi:10.1016/j.dsr2.2008.10.037.
- Gordon, A.L., Padman, L., Bergamasco, A., 2009b. Southern Ocean shelf slope exchange. *Deep-Sea Research Part II* 56, 775–777. doi:10.1016/j.dsr2.2008.11.002.
- Grinsted, A., Moore, J.C., Jevrejeva, S., 2004. Application of the cross wavelet transform and wavelet coherence to geophysical time series. *Nonlinear Processes in Geophysics* 11, 561–566.
- Holland, D.M., Jacobs, S.S., Jenkins, A., 2003. Modelling the ocean circulation beneath the Ross Ice Shelf. *Antarctic Science* 15 (1), 13–23. doi:10.1017/S0954102003001019.
- Ivanov, V.V., Shapiro, G.I., Huthnance, J.M., Aleynik, D.L., Golovin, P.N., 2004. Cascades of dense water around the world ocean. *Progress in Oceanography* 60, 47–98.
- Jackett, D.R., McDougall, T.J., 1997. A neutral density variable for the world's oceans. *Journal of Physical Oceanography* 27 (2), 237–263.
- Jacobs, S.S., 2004. Bottom water production and its links with the thermohaline circulation. *Antarctic Science* 16, 427–437.
- Jacobs, S.A., Fairbanks, R.C., Horibe, Y., 1985. Origin and evolution of water masses near the Antarctic continental margin: evidence from H21802/H21602 ratios in seawater. In: Jacobs, S.S. (Ed.), *Oceanology of the Antarctic Continental Shelf*, vol. 3, pp. 59–85.
- Jacobs, S.S., Giulivi, C.F., Mele, P.A., 2002. Freshening of the Ross Sea during the late 20th century. *Science* 297, 386–389.
- Jacobs, S.S., Giulivi, C.F., 2010. Large multidecadal salinity trends near the Pacific–Antarctic continental margin. *Journal of Climate* 23, 4508–4524.
- Jaeger, J.M., Nittrouer, C.A., DeMaster, D.J., Kelchner, C., Dunbar, R.B., 1996. Lateral transport of settling particles in the Ross Sea and implications for the fate of biogenic material. *Journal of Geophysical Research* 101, 18479–18488.
- Johnson, G.C., 2008. *Quantifying Antarctic Bottom Water and North Atlantic Deep Water volumes*. *Journal of Geophysical Research* 113, C05027. doi:10.1029/2007JC004477.
- Johnson, E.S., Van Woert, M.L., 2006. Tidal currents of the Ross Sea and their time stability. *Antarctic Science* 18 (1), 141–154.
- Killworth, P.D., 1977. Mixing on the Weddell Sea continental slope. *Deep-Sea Research* 24, 427–448.
- Legg, S., et al., 2009. Improving oceanic overflow representation in climate models: the gravity current entrainment climate process team. *Bulletin of the American Meteorological Society* 90, 657–670. doi:10.1175/2008BAMS2667.1.
- Locarnini, R.A., 1994. *Water masses and circulation in the Ross Gyre and environs*. PhD thesis, Texas A&M University, 87 pp. [Unpublished].
- Long, R.R., 1954. Some aspects of the flow of stratified fluids: II. Experiments with a two-fluid system. *Tellus* 2, 97–115.
- Meyers, S.D., Keu, B.G., O'Brien, J., 1993. An introduction to wavelet analysis in oceanography and meteorology: with application to the dispersion of Yanai waves. *Monthly Weather Review* 121 (10), 2858–2866.
- Morlet, J., Arens, G., Forgeau, I., Giard, D., 1982. Wave propagation and sampling theory. *Geophysics* 47, 203–236.

- Morlet, J., 1983. Sampling theory and wave propagation. Acoustic Signal/image Processing and recognition. In: Chen, C.H. (Ed.), NATO ASI Series, 1. Springer Verlag, pp. 233–261.
- Muench, R.D., Padman, L., Gordon, A.L., Orsi, A.H., 2009a. Mixing of a dense water outflow from the Ross Sea, Antarctica: the contribution of tides. *Journal of Marine Systems*. doi:10.1016/j.jmarsys.2008.11.003.
- Muench, R., Wählin, A., Özgökmen, T., Hallberg, R., Padman, L., 2009b. Impacts of bottom corrugations on a dense Antarctic outflow: the NW Ross Sea. *Geophysical Research Letters* 36, 23. doi:10.1029/2009GL01347.
- Orsi, A.H., Johnson, G.C., Bullister, J.L., 1999. Circulation, mixing, and production of Antarctic Bottom Water. *Progress in Oceanography* 43, 55–109.
- Orsi, A.H., Jacobs, S.S., Gordon, A.L., Visbeck, M., 2001. Cooling and ventilating the abyssal ocean. *Geophysical Research Letters* 28 (15), 2923–2926.
- Orsi, A.H., Smethie Jr., W.M., Bullister, J.L., 2002. On the total input of Antarctic waters to the deep ocean: a preliminary estimate from chlorofluorocarbon measurements. *Journal of Geophysical Research* 107 (C8), 3122. doi:10.1029/2001JC000976.
- Orsi, A.H., Wiederwohl, C.L., 2009. A recount of Ross Sea waters. In: Gordon, A., Padman, L., Bergamasco, A. (Eds.), *Deep-Sea Research Part II. Southern Ocean Shelf Slope Exchange*. doi:10.1016/j.dsr2.2008.10.033.
- Ozaki, H., Obata, H., Naganobu, M., Gamou, T., 2009. Long-term bottom water warming in the north Ross Sea. *Journal of Oceanography* 65 (2), 235. doi:10.1007/s10872-009-0022-z.
- Padman, L., Howard, S., Orsi, A., Muench, R., 2009. Tides of the northwestern Ross Sea and their impact on dense outflows of high salinity shelf water. In: Gordon, A., Padman, L., Bergamasco, A. (Eds.), *Deep-Sea Research Part II. Southern Ocean Shelf Slope Exchange*. doi:10.1016/j.dsr2.2008.10.026.
- Pawlowicz, R., Beardsley, B., Lentz, S., 2002. Classical tidal harmonic analysis including error estimates in MATLAB using T TIDE. *Computers & Geosciences* 28, 929–937.
- Rintoul, S.R., 1998. On the origin and influence of Adelie Land Bottom Water. In: Jacobs, S., Weiss, R. (Eds.), *Ocean, Ice and Atmosphere: Interactions at the Antarctic Continental Margin*. Antarctic Research Series, vol. 75. American Geophysical Union, Washington, DC, pp. 151–171.
- Rintoul, S.R., 2007. Rapid freshening of Antarctic Bottom Water formed in the Indian and Pacific oceans. *Geophysical Research Letters* 34, L06606. doi:10.1029/2006GL028550.
- Rivarolo, P., Frache, R., Bergamasco, A., Hohmann, R., 2003. Dissolved oxygen, NO and PO as tracers for Ross Sea Ice Shelf Water overflow. *Antarctic Science* 15, 399–404.
- Robertson, R., 2005. Baroclinic and barotropic tides in the Ross Sea. *Antarctic Science* 17, 107–120.
- Robertson, R., Visbeck, M., Gordon, A.L., Fahrbach, E., 2002. Long-term temperature trends in the deep waters of the Weddell Sea. *Deep-Sea Research II* 49, 4791–4806.
- Rubino, A., Budillon, G., Pierini, S., Spezie, G., 2003. A model for the spreading and sinking of the deep Ice Shelf water in the Ross Sea. *Antarctic Science* 15 (1), 25–30.
- Rusciano, E., Budillon, G., Spezie, G., Bergamasco, A., Aliani, S., Capello, M., 2008. Interannual Variability of High Salinity Shelf Water Production from Terra Nova Bay Polynya. Biennial SCAR Meeting, 87–12 July, San Petersburg, Russia.
- Russo, A., 1999. Water mass characteristics during the ROSSMIZE Cruise (western sector of the Ross Sea, November–December 1994). In: Spezie, G., Manzella, G.M.R. (Eds.), *Oceanography of the Ross Sea*. Springer, Antarctica, Berlin, pp. 83–93.
- Shapiro, G.I., Hill, A.E., 1997. Dynamics of dense water cascades at the shelf edge. *Journal of Physical Oceanography* 27, 2381–2394.
- Shapiro, G.I., Huthnance, J.M., Ivanov, V.V., 2003. Dense water cascading off the continental shelf. *Journal of Geophysical Research* 108 (C12) art no. 3390.
- Smedsrud, L.H., 2005. Warming of the deep water in the Weddell Sea along the Greenwich meridian: 1977–2001. *Deep-Sea Research I* 52, 241–258.
- Smethie Jr., W.M., Jacobs, S.S., 2005. Circulation and melting under the Ross Ice Shelf: estimates from evolving CFC, salinity and temperature fields in the Ross Sea. *Deep-Sea Research I* 52, 959–978.
- Smith Jr, W.O., Shields, A.R., Peloquin, J.A., Catalano, G., Tozzi, S., Dinniman, M.S., Asper, V.A., 2006. Interannual variations in nutrients, net community production, and biogeochemical cycles in the Ross Sea. *Deep-Sea Research II* 53, 815–833.
- Stacey, M.W., Bowen, A.J., 1988. The vertical structure of density and turbidity currents: theory and observations. *Journal of Geophysical Research* 93, 3528–3542.
- Trumbore, S.E., Jacobs, S.S., Smethie Jr., W.M., 1991. Chlorofluorocarbon evidence for rapid ventilation of the Ross Sea. *Deep-Sea Research* 38 (7), 845–870.
- UNESCO, 1983. The acquisition, calibration and analysis of CTD data. A report of SCOR WG 51. *Technical Papers in Marine Science*, pp. 54–59.
- UNESCO, 1988. Algorithms for Computation of Fundamental Properties of Seawater. *Technical Papers in Marine Science*, pp. 44–53.
- Wang, Q., Danilov, S., Hellmer, H.H., Schröter, J., 2010. Overflow dynamics and bottom water formation in the western Ross Sea: influence of tides. *Journal of Geophysical Research* 115, C10054. doi:10.1029/2010JC006189.
- Wang, Q., Danilov, S., Schröter, J., 2009. Bottom water formation in the southern Weddell Sea and the influence of submarine ridges: idealized numerical solutions. *Ocean Modelling* 28, 50–59. doi:10.1016/j.ocemod.2008.08.003.
- Whitworth, T., Orsi, A.H., Kim, S.-J., Nowlin Jr, W.D., Locarnini, R.A., 1998. Water masses and mixing near the Antarctic Slope Front. *Antarctic Research Series* 75, 1–27.
- Whitworth, T., Orsi, A.H., 2006. Antarctic Bottom Water production and export by tides in the Ross Sea. *Geophysical Research Letters* 33, L12609. doi:10.1029/2006GL026357.
- Visbeck, M., 2001. Deep velocity profiling using lowered acoustic Doppler current profilers: bottom track and inverse solutions. *Journal of Atmospheric and Oceanic Technology* 19, 794–807.
- Visbeck, M., Thurnherr, A.M., 2009. High resolution velocity and hydrographic observations of the Drygalski trough gravity plume. In: Gordon, A., Padman, L., Bergamasco, A. (Eds.), *Deep-Sea Research Part II. Southern Ocean Shelf Slope Exchange*. doi:10.1016/j.dsr2.2008.10.029.